## Nano-Micro Letters

REVIEW

https://doi.org/10.1007/s40820-025-01916-9



Cite as Nano-Micro Lett. (2026) 18:82

Received: 7 June 2025 Accepted: 12 August 2025 © The Author(s) 2025

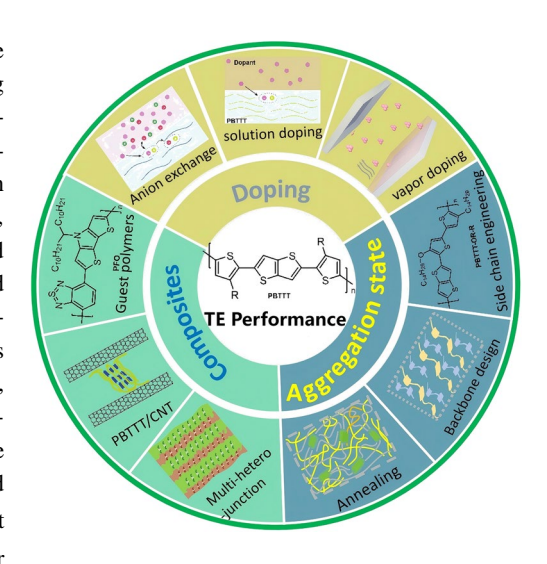
## An Emerging Liquid-Crystalline Conducting Polymer Thermoelectrics: Opportunities and Challenges

Zhenqiang Ye<sup>1</sup>, Mingdong Zhang<sup>1</sup>, Junyang Deng<sup>1</sup>, Lirong Liang<sup>1</sup>, Chunyu Du<sup>1</sup>, Guangming Chen<sup>1</sup>

#### HIGHLIGHTS

- Poly(2,5-bis(3-alkylthiophen-2-yl)thieno[3,2-b]thiophene) (PBTTT) synthesis and main strategies to enhance its thermoelectric performance (including doping, composite engineering and aggregation state controlling) are comprehensively reviewed.
- The thermoelectric performances of PBTTT-related materials are systematically summarized and compared.
- Future opportunities of PBTTT thermoelectric performance enhancement and effective utilization of its unique melt processibility in multiscale regulation, composite and hybrid, and processing technology innovation are outlooked.

ABSTRACT Thermoelectric (TE) materials, being capable of converting waste heat into electricity, are pivotal for sustainable energy solutions. Among emerging TE materials, organic TE materials, particularly conjugated polymers, are gaining prominence due to their unique combination of mechanical flexibility, environmental compatibility, and solution-processable fabrication. A notable candidate in this field is poly(2,5-bis(3-alkylthiophen-2-yl)thieno[3,2-b]thiophene) (PBTTT), a liquid-crystalline conjugated polymer, with high charge carrier mobility and adaptability to melt-processing techniques. Recent advancements have propelled PBTTT's figure of merit from below 0.1 to a remarkable 1.28 at 368 K, showcasing its potential for practical applications. This review systematically examines strategies to enhance PBTTT's TE performance through doping (solution, vapor, and anion exchange doping), composite engineering, and aggregation state controlling. Recent key breakthroughs include ion exchange doping for stable charge modulation, multi-heterojunction architectures reducing thermal conductivity, and proton-coupled electron transfer doping for precise Fermi-level tuning. Despite great progress, challenges still persist in enhancing TE conversion efficiency, balancing or



decoupling electrical conductivity, Seebeck coefficient and thermal conductivity, and leveraging melt-processing scalability of PBTTT. By bridging fundamental insights with applied research, this work provides a roadmap for advancing PBTTT-based TE materials toward efficient energy harvesting and wearable electronics.

KEYWORDS Thermoelectric materials; Polymer; PBTTT; Liquid-crystalline

<sup>&</sup>lt;sup>1</sup> College of Materials Science and Engineering, Shenzhen University, Shenzhen 518055, People's Republic of China





<sup>☐</sup> Guangming Chen, chengm@szu.edu.cn

### 1 Introduction

82

With growing global focus on sustainable development and carbon emission reduction, research on energy recovery and re-utilization has witnessed explosive advances [1]. Based on the Seebeck effect, a temperature difference across a material generates an electric potential by driving charge carriers from hot to cold regions, thermoelectric (TE) technology [2, 3] can directly and effectively convert heat to electrical energy and vice versa, thereby being effective in the recovery of waste heat and low-grade heat and displaying promising prospects in achieving low-carbon economy. The development of high-performance TE materials is vital. Historically, inorganic TE materials, such as bismuth telluride (Bi<sub>2</sub>Te<sub>3</sub>) [4], lead telluride (PbTe) [5] and tin selenide (SnSe) [6], have been extensively investigated. However, their disadvantages, including toxicity, low content in earth, high intrinsic rigidity and inevitable elevated energy consumption during processing, seriously limit their large-scale applications [7, 8]. Fortunately, the recently-developed organic counterparts [9, 10] reveal distinct advantages, covering low cost, exceptional flexibility [11, 12], facile processing [13–16], and eco-friendly non-toxicity [17, 18], which have garnered much of current interest. Notably, they have enabled diverse applications including artificial intelligence [19, 20], fire recognition and alarming [21–23], smart buildings [24, 25], wearable and flexible electronics [26–28]. So far, conjugated polymers [29, 30] represent the most extensively studied class of organic TE (OTE), being characteristic of their intrinsic conjugated  $\pi$ -electron systems that confer remarkable electronic properties [31–33]. The development of conjugated polymers can be traced back to 1977 [34]. Polyacetylene (PA) belongs to the first generation, possessing ultra-high conductivity [35]. However, air instability and processability limitations hindered its development. Subsequently, various conjugated polymers have been reported, such as polythiophene (PTh) [36, 37], polyaniline (PANI) [38, 39], polypyrrole (PPy) [40, 41], poly(3-hexylthiophene) (P3HT) [42, 43], and poly-(3,4-ethylene dioxythiophene) (PEDOT) [44-47].

In recent years, a class of conjugated polymers with liquid-crystalline phases, poly(2,5-bis(3-alkylthiophen-2-yl) thieno[3,2-b] thiophenes) (PBTTT) [48], has attracted increasing attention due to its unique molecular structure and excellent performance. As shown in Table 1, compared

to these common TE polymers, PBTTT exhibits distinct advantages. Firstly, it possesses a rigid and highly conjugated backbone, which facilitates efficient charge transport and thereby significantly enhances the carrier mobility. Secondly, it has high-temperature stability and can be prepared using melt-processing technology. More importantly, PBTTT exhibits liquid-crystalline behavior through selfassembly of its extended thiophene backbones into highly ordered lamellar structures. This liquid-crystalline microstructure facilitates anisotropic charge transport properties critical for TE performance. The resulting long-range ordered domains emerge from solution processing, enabling efficient  $\pi$ – $\pi$  stacking that enhances carrier mobility. Hence, PBTTT demonstrates versatile potentials in wide applications, including organic field-effect transistors [49, 50], organic photodetectors [51, 52], organic photovoltaics [53, 54], light-emitting diodes [55, 56], and TE devices [57, 58]. A recent study published by Jin et al. unveiled a PBTTTbased TE material that achieved a figure of merit of 1.28 at 368 K [59], clearly underscoring its promising potential for TE applications. So far, researchers have actively explored extensive strategies to enhance the TE performance of PBTTT. As illustrated in Fig. 1, these approaches encompass chemical doping to optimize charge carrier concentration and mobility, aggregation state regulation to fine-tune molecular ordering and crystallinity, and the development of composite materials that synergistically combine PBTTT with other functional components. Each of these methods has demonstrated unique potential in addressing the intrinsic limitations of PBTTT, paving the way for its promising prospects in next-generation TEs.

Despite significant advancements in PBTTT research for TE applications, a systematic review, covering the latest developments is strongly desired for this cutting-edge field. The most recent related review, published by our group in 2021 [60], can no longer reflect the current advances. Here, we aim to comprehensively summarize recent achievements in improving the TE performance of PBTTT, systematically compare the advantages and disadvantages of present approaches, and establish connections among various strategies to provide theoretical guidance and technical support for further optimization of PBTTT's TE performance. In the first section, we will systematically introduce the synthesis strategies of PBTTT and its derivatives, as well as film fabrication techniques, with particular emphasis on solution-processed approaches that represent

Table 1 Comparison of PBTTT with other polymer TE materials

	Structural characteristics	TE properties		Processability	
		$\overline{\sigma}$	S		
PEDOT:PSS	Rigid conjugation	High	Low	Solution	
PTh	Linear conjugation	Medium	High	Vapor deposition	
PANI	Weak conjugation	Low	Medium	Solution In-situ polymerization	
PPy	Non-planar conjugation	Medium	Medium	Electrodeposition	
PBTTT	Rigid conjugation Liquid-crystalline phases	High	Medium–High	Solution Melt	

the most prevalent form for practical applications. Then, we focus on discussing several representative approaches to enhancing TE performance. Subsequently, we provide a comprehensive discussion of the latest research advancements in PBTTT TE materials. Finally, based on the current research landscape, we offer an outlook on the future development trends of PBTTT and delve into the potential breakthrough directions for its TE properties. This review will offer researchers a comprehensive reference framework and promote the practical applications of PBTTT in TE materials.

#### 2 Fabrication

#### 2.1 Synthesis Method of PBTTT and Its Derivatives

McCulloch and colleagues proposed the synthesis of PBTTT based on a microwave-assisted Stille coupling reaction, being an important method to synthesize polythiophenes [61]. The Stille coupling reaction has become a widely used coupling reaction in organic synthesis. In the reaction, organotin compounds are coupled with halogenated alkanes or aromatic compounds under Pd catalysis [62, 63]. An exchange reaction between organotin compounds and halogenated species can facilitate the formation of new carbon-carbon bonds. The term "microwave-assisted" refers to the use of microwave radiation as an alternative to conventional heating methods. To date, microwave-assisted synthesis has been widely adopted in organic chemistry [61], primarily due to its significant advantages over traditional thermal approaches, including dramatically accelerated reaction rates along with higher product yields and reduced byproduct formation.

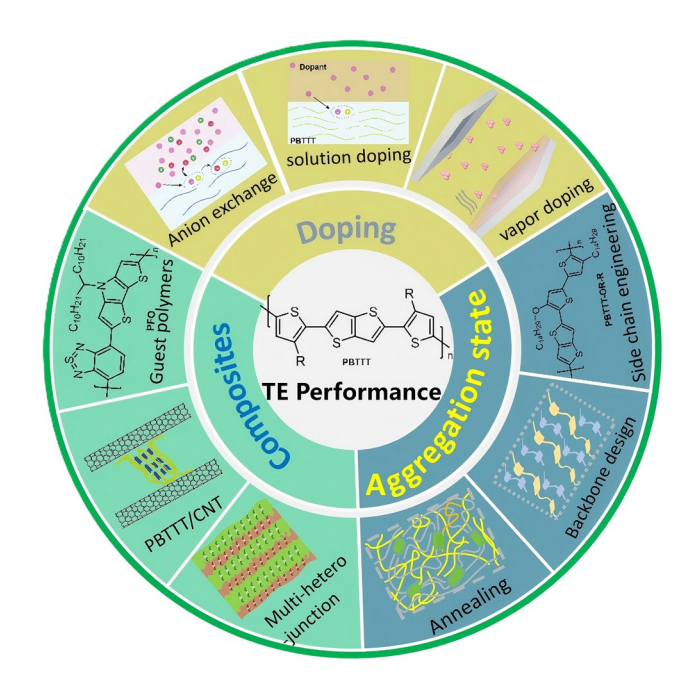


Fig. 1 An overview of methods to enhance TE properties of PBTTT

As a highly designable conjugated polymer, PBTTT enables precise tailoring of material properties through rational side-chain engineering. Recent studies demonstrate that strategically modifying side-chain architecture allows effective controls intra/interchain interactions to enhance TE performance. Researchers have developed various PBTTT derivatives with functionalized side chains. Durand et al. [64] synthesized PBTTT- $^{x}$ O derivatives featuring single-etherbased side chains (x=3, 5, 8, 11) and demonstrated that the single-ether moiety enhanced polymer/dopant interactions while simultaneously maintaining PBTTT's advantageous lamellar structure. Okamoto and coworkers [65] synthesized two PBTTT isomers with alkoxy (icosyl) side chains





at distinct positions, PBTTT- $(OC_{20})_2$  and PBTTT-i- $(OC_{20})_2$  (Fig. 2a). These alkoxy substituents enhanced backbone rigidity through intramolecular non-covalent S···O interactions while elevating the highest-occupied-molecular-orbital (HOMO) energy levels compared to their alkyl counterparts. Subsequent study by Chen's group [66] revealed that biaxial conjugated scaffolds with thienyl-ester functionalities could amplify charge transport properties under mechanical strain, achieving carrier mobility enhancements of up to threefold through ester-modified topological control.

82

However, the conventional Stille coupling approach for PBTTT derivatives often suffers from substantial homocoupling defects. To address this issue, Vanderspikken et al. [67] developed a symmetric oxidative polymerization method that effectively mitigated such defects. Subsequently, Goderis and coworkers [68] successfully extended this strategy to synthesize the PBTTT-OR-R derivative, previously regarded as highly desirable for its performance characteristics. For comparative evaluation, classical Stille cross-coupling was also employed to prepare the same polymer (Fig. 2b, c). Structural analyses demonstrated that the oxidative polymerization-derived PBTTT-OR-R exhibited superior chemical stability compared to its Stille-coupled counterpart.

#### 2.2 Fabrication Methods of PBTTT Films

Solution processing is the primary manufacturing approach for conjugated polymers. Typical solution processing techniques (Fig. 3a) for PBTTT encompass spin coating [69–71], drop casting [72], dip casting [73] and blade coating [74, 75]. Spin coating deposits a PBTTT solution onto a substrate, which is rapidly spun to form a film. However, spincoated films typically exhibit disordered molecular packing, requiring post-deposition thermal annealing to improve crystallinity. Drop casting is simple, involving natural drying of a solution on a substrate. Nevertheless, it often produces films with poor uniformity and uncontrollable thickness. Dip coating involves immersing a substrate into a precursor solution and withdrawing it at a controlled rate. The resulting film morphology is highly dependent on withdrawal speed, solution concentration, viscosity, immersion time and withdrawal angle, affording reproducibility challenging. Blade coating applies shear forces to align molecules by spreading ink uniformly across a substrate using a bladed applicator, which often yields better molecular alignment than spin coating due to induced directional shear.

In addition to traditional fabrication methods, various innovative thin-film deposition techniques have been developed, displaying distinct characteristics and unique advantages.

### 2.2.1 Floating Film Transfer Method (FTM)

The FTM technique, proposed by Takashima's research group [76–78] (Fig. 3b), represents a novel thin-film fabrication method based on liquid-interface self-assembly mechanisms. This approach ingeniously exploits the Marangoni effect, driven by surface tension gradients: when a PBTTT solution is drop-cast onto a liquid substrate, the rapid evaporation of solvent generates a concentration gradient, and induces radial fluid flow that facilitates uniform spreading. This method combines operational simplicity and low-cost fabrication, achieving both near-100% material utilization efficiency and the formation of high-quality and uniform thickness films.

## 2.2.2 Hyper 100 °C Langmuir-Blodgett (LB) Technique

Watanabe's team [79] developed the Hyper 100 °C LB technique (Fig. 3c), successfully overcoming the limitations of conventional LB methods for amphiphilic molecules. By employing high-boiling-point solvents (e.g., ethylene glycol, boiling point 197 °C) or ionic liquids (boiling point > 300 °C) as the subphase, they achieved ordered monolayer transfer of PBTTT onto substrates via horizontal lifting at elevated temperatures (80–140 °C). This modified approach not only eliminates molecular misalignment caused by vertical lifting, but also significantly enhances film uniformity. More importantly, edge-on molecular packing mode is generated to facilitate efficient charge transport, a configuration where the  $\pi$ -conjugated backbone planes of the polymer chains are perpendicular to the substrate. In contrast, the face-on orientation features  $\pi$ -conjugated backbone planes parallel to the substrate.

#### 2.2.3 Nozzle Printing Method

The nozzle printing fabrication technique developed by Boseok Kang's team [80] achieved seamless integration of Nano-Micro Lett. (2026) 18:82 Page 5 of 34 82

Fig. 2 Synthesis methods of PBTTT derivatives. a Synthesis methods of PBTTT- $(OC_{20})_2$  and PBTTT- $(OC_{20})_2$  [65]. b PBTTT-OR-R synthesized by the Stille cross-coupling approach [68]. c PBTTT-OR-R synthesized by the symmetric oxidative polymerization approach [68]

thin-film preparation and printing processes. They employed triphenylsulfonium triflate (TPS-TF) as a photoactivated dopant, which remains chemically inert in solution and only initiates solid-state doping reactions upon UV exposure. By leveraging this mechanism, the technique effectively circumvents issues inherent to conventional dopants, such as solution aggregation and printhead clogging, while enabling quantitative control of carrier concentration through precise UV exposure time modulation.

## 2.2.4 Physical Supercritical Fluid Deposition (p-SFD)

Kaake and coworkers [81] devised the p-SFD technique employing n-pentane (critical temperature: 196.6 °C, critical pressure: 3.37 MPa) as an inert supercritical medium to deposit polymer films through pressure-regulated phase transitions. By precisely controlling working pressure and solvent additive composition, this method enables the flexible fabrication of films with either nanowire structures or uniform smoothness. Although this green





82 Page 6 of 34 Nano-Micro Lett. (2026) 18:82

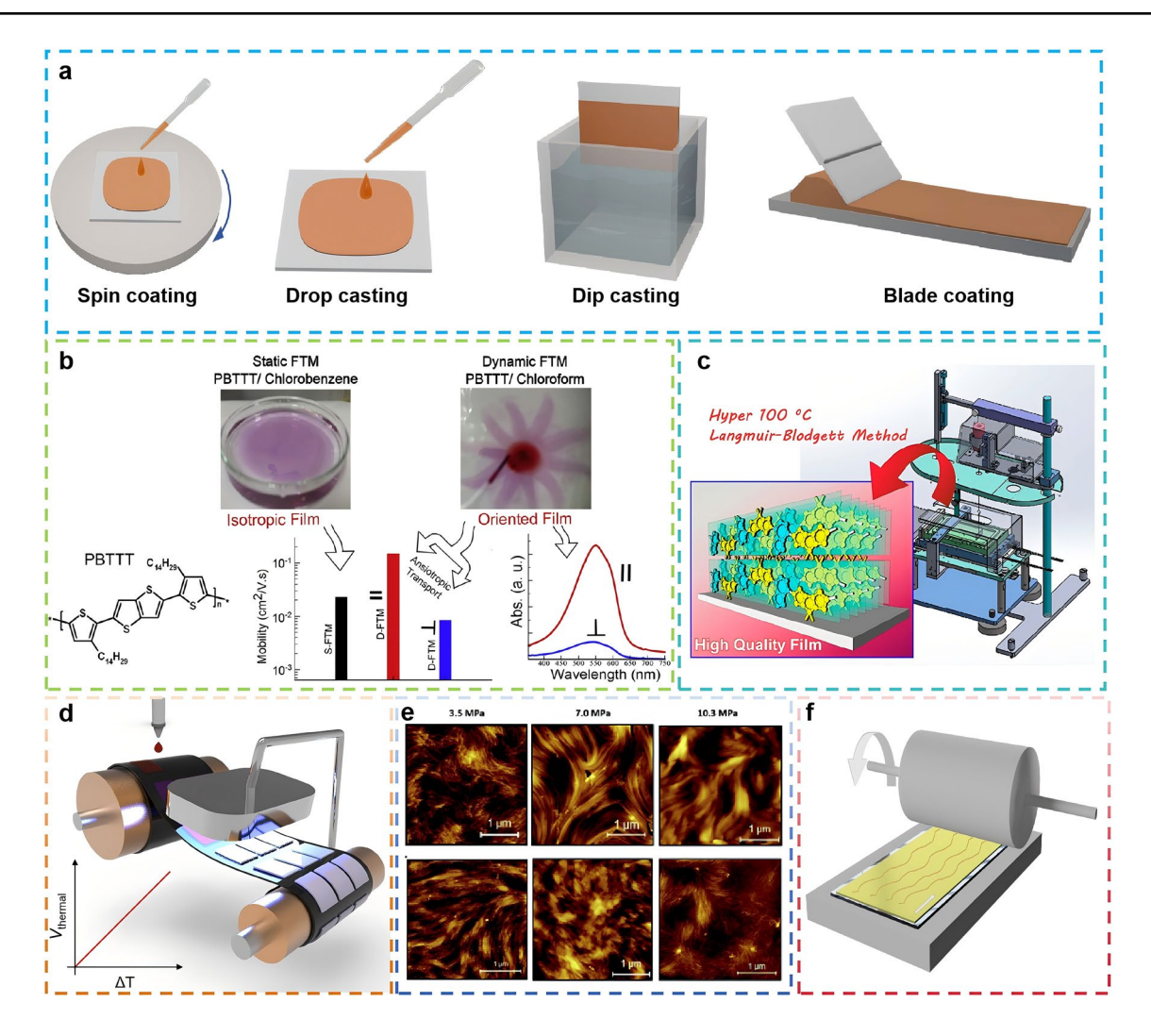


**Fig. 3** Processing methods for PBTTT films. **a** Traditional processing method, including spin coating, drop casting, dip casting and blade coating. **b** Schematic of floating film transfer method [76]. **c** Schematic of hyper 100 °C LB method [79]. **d** Schematic of nozzle printing [80]. **e** AFM images of PBTTT-C<sub>14</sub> films formed in supercritical fluids under different pressure [81]. **f** Schematic of alignment by high-T rubbing [82]

fabrication technique demonstrates promising application potential, its industrialization still faces key challenges, including equipment costs and process standardization.

#### 2.2.5 High Temperature Rubbing (High-T Rubbing)

Based on the unique thermotropic liquid-crystalline behavior of PBTTT within the temperature range of 140–180 °C, the Brinkmann research group proposed an efficient high-T rubbing [82] alignment technique. Within this characteristic temperature window, PBTTT polymer

chains exist in a dynamically ordered state, where the melting of side chains reduces intermolecular steric hindrance, enabling long-range alignment of backbone chains under shear forces. By precisely controlling rubbing temperature and shear rate, this method effectively overcomes van der Waals interactions, guiding PBTTT polymer chains to align along the rubbing direction, thereby forming well-ordered  $\pi$ - $\pi$  stacking structures with mixed face-on/edge-on crystalline domains. This solvent-free solid-state alignment technique has demonstrated several advantages, including compatibility with roll-to-roll continuous manufacturing, shorter processing time compared to traditional epitaxial growth methods,

and the ability to achieve uniaxial alignment films on conventional glass/plastic substrates without requiring single-crystal templates.

These fabrication strategies not only broaden the processing approaches for PBTTT films, but also offer versatile technological alternatives for performance enhancement and industrial manufacturing of organic electronic devices, marking a promising developmental trajectory in materials processing science.

# 3 Strategies for Enhancement of TE Properties

The most important TE performance indicator is the figure of merit (ZT), which is expressed as:

$$ZT = \frac{S^2 \sigma}{\kappa} T \tag{1}$$

where S denotes the Seebeck coefficient,  $\sigma$  is the electrical conductivity, and  $S^2\sigma$  is called power factor (PF). T is the temperature, and  $\kappa$  is thermal conductivity. Over years of development, the ZT of PBTTT has significantly improved from an initial value of far below 0.1 to approximately 1.28 at 368 K [59]. This remarkable enhancement has been achieved through optimized strategies addressing three key parameters:  $\sigma$ , S, and  $\kappa$ . Below, we summarize the typical strategies for enhancement of TE properties.

#### 3.1 Doping

Doping represents a cornerstone strategy to optimize TE performance in conjugated polymers. Controlled dopant incorporation enables precise modulation of charge carrier density and crystallinity, directly optimizing key TE parameters, including  $\sigma$ , S, and  $\kappa$ .

#### 3.1.1 Dopants for PBTTT

In available literatures, PBTTT has been mainly studied in the context of p-type doping due to its favorable hole transport properties. Figure 4a–c displays different types of dopants typically employed in PBTTT. The doping mechanism fundamentally relies on redox-driven charge transfer, facilitated by favorable energy-level alignment between the dopant and the host material. As such, the p-doped PBTTT

systems typically employ strong electron-accepting dopants whose energy levels complement those of PBTTT [83], such as 2,3,5,6-tetrafluorotetracyanoquinodimethane ( $F_4$ TCNQ) [58, 84, 85], 1,3,4,5,7,8-hexafluoro-tetracyano-naphtho-quinodimethane ( $F_6$ TCNNQ) [82], and ferric chloride FeCl<sub>3</sub> [75].

Recent studies have expanded doping strategies to include acid–base chemistry as an alternative to traditional redox-based methods. Among these, the Lewis acid tris(pentafluorophenyl)borane (BCF) [73, 86, 87] has emerged as a particularly promising dopant (Fig. 4d). Its hydrated form, BCF-water, further acts as a strong Brønsted acid, enabling efficient proton-mediated doping. Compared to conventional electron acceptors like  $F_4TCNQ$ , BCF offers superior solubility in various organic solvents, facilitating homogeneous doping and improved charge transfer efficiency. Recent work has successfully demonstrated BCF as an effective p-type dopant for PBTTT, achieving high  $\sigma$  and excellent charge transport properties.

Since high doping concentrations can degrade the material's microstructure and stability by disrupting the  $\pi$ - $\pi$  stacking of polymer chains, thereby negatively impacting conductivity, Brinkmann et al. employed tris(4-bromophenyl) ammoniumyl hexachloroantimonate as a dopant, commonly known as Magic Blue (MB) [88-90] (Fig. 4e). MB preferentially localizes in the amorphous regions of PBTTT, while charge carriers (holes) predominantly concentrate within the crystalline domains. Crucially, the crystalline phase remains undoped, preserving its high charge carrier mobility. In contrast, conventional dopants such as F<sub>4</sub>TCNQ and F<sub>6</sub>TCNNQ intercalate into the side-chain layers of the crystalline phase, disrupting the critical  $\pi$ - $\pi$  stacking and consequently reducing conductivity. Remarkably, this strategy achieved an exceptional conductivity of 9700 S cm<sup>-1</sup> with MB doping [88], significantly outperforming F<sub>6</sub>TCNNQ-doped samples which showed only 2430 S cm<sup>-1</sup>.

In addition, ionic liquids (ILs) [91–94] have proven to be highly effective dopants for conjugated polymers due to their exceptional properties, including superior environmental stability, broad solvent compatibility, and the ability to facilitate ion–electron coupled transport while minimizing structural disruption to crystalline domains. ILs consist of cation–anion pairs, where the anion acts as an oxidizing agent, enabling p-doping via charge transfer, while the cation provides an ion-conductive medium, enhancing ion diffusion. Tanaka et al. [92] developed





82 Page 8 of 34 Nano-Micro Lett. (2026) 18:82

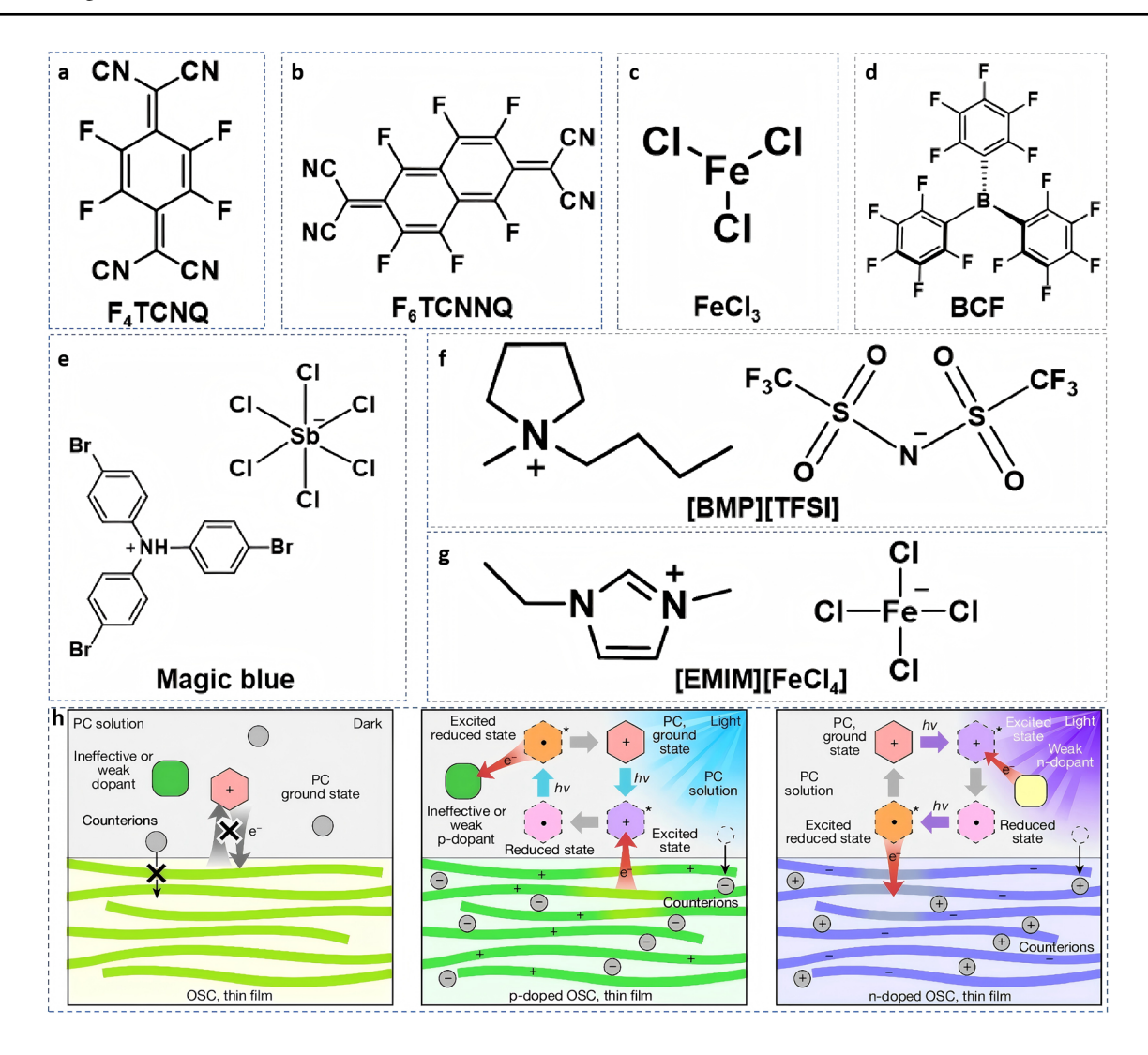


Fig. 4 a-g Typical dopants for PBTTT, including F<sub>4</sub>TCNQ, F<sub>6</sub>TCNNQ, FeCl<sub>3</sub>, BCF, MB, and ILs. **h** Schematics of the photocatalytic doping processes [95]

an IL-based chemical doping strategy using [1-ethyl-3-methylimidazolium (EMIM)][FeCl<sub>4</sub>] (Fig. 4e). X-ray diffraction (XRD) confirmed the retention of high crystallinity after IL doping, avoiding the structural degradation typically induced by conventional dopants. Sirringhaus and colleagues [93] employed a synergistic doping strategy through the combination of [1-butyl-1-methylpyrrolidinium] [bis(trifluoromethanesulfonyl)imide] ([BMP][TFSI]) (Fig. 4g) with FeCl<sub>3</sub>, which not only enhanced doping efficiency but also maintained PBTTT crystallinity while exhibiting minimal structural degradation.

A recent study published in Nature [95] introduces a photocatalytic doping approach for organic semiconductors,

where oxygen serves as a mild p-type dopant. In Fig. 4h, the method employs photocatalysts, which, upon light excitation, extract electrons from conductive polymers, undergo self-reduction, and are subsequently regenerated by O<sub>2</sub>. Unlike conventional doping methods that often disrupt crystallinity, this strategy maintains thin-film molecular ordering and crystallinity during the doping process. Their approach can operate under mild and environmentally benign conditions, enabling reactions to proceed at room temperature in ambient air. Remarkably, only trace amounts of salts are consumed to maintain charge neutrality, while the photocatalysts remain fully recyclable, minimizing chemical waste and enhancing process sustainability.

#### 3.1.2 Doping Methods

Doping methods can be systematically classified based on their implementation strategies, with the most extensively studied approaches encompassing: Solution doping [58, 92, 96, 97] and vapor doping [72, 84]. Most recently, anion exchange doping [85, 93, 94] has been recognized as an advancement in doping technology, offering unique advantages in terms of tunable charge carrier density and material stability. Solution doping is a processing technique that introduces dopant into a host material by codissolving both components in a common solvent. This method features straightforward operation and demonstrates excellent compatibility with broader manufacturing processes. Vapor doping is a dry-phase processing technique where gaseous dopant diffuse into solid-state materials, enabling precise control over dopant concentration and penetration depth. Anion exchange is an electrochemical process where mobile ions in a solution are reversibly substituted with counterions bound to a solid material (ion exchanger). This occurs via electrostatic interactions while preserving charge neutrality.

3.1.2.1 Solution Doping Solution doping remains the most prevalent doping approach due to its operational simplicity. However, achieving effective carrier generation typically necessitates high dopant loadings that compromise the crystalline integrity of PBTTT, a trade-off that fundamentally limits TE performance. Solution-sequential (SSq) doping was designed specifically to decouple dopant diffusion from crystallization kinetics [58, 92, 97], wherein dopants are introduced to pre-deposited PBTTT films rather than blended directly in solution. Kilwon Cho et al. [58] employed SSq doping to incorporate F<sub>4</sub>TCNQ into PBTTT, achieving a maximum dopant concentration of 20 mg mL<sup>-1</sup> with a resulting conductivity of 13 S cm<sup>-1</sup>. However, a key limitation persists: The restricted infiltration of F<sub>4</sub>TCNQ into the crystalline domains of PBTTT constrains doping efficiency and ultimately caps conductivity enhancement.

Subsequently, Brinkmann and coworkers [96] introduced an incremental concentration doping (ICD) strategy, systematically comparing the performance of two common p-type dopants, F<sub>4</sub>TCNQ and F<sub>6</sub>TCNNQ. As illustrated in Fig. 5a, the ICD method employs sequential, stepwise immersion into solutions with progressively increasing dopant concentrations, whereas direct doping (DD) utilizes single-step immersion; this gradual ICD approach

minimizes disruptions to PBTTT's molecular order, preserving high charge carrier mobility while enabling deeper and more uniform dopant penetration into crystalline domains. However, this method yields limited TE enhancement for dopants with excessive diffusion rates. As shown in Fig. 5b, F<sub>4</sub>TCNQ demonstrated high diffusivity, being 4.5 times greater than that of F<sub>6</sub>TCNNQ, resulting in disordered dopant arrangements under ICD treatment; conversely, the larger molecular dimensions of F<sub>6</sub>TCNNQ facilitated ordered alignment. Consequently, ICD substantially enhanced TE performance for F<sub>6</sub>TCNNQ compared to DD. Figure 5c, d directly quantifies these performance gains: ICD achieved a 114% PF improvement for F<sub>6</sub>TCNNQ versus a marginal 18% increase for F<sub>4</sub>TCNQ.

3.1.2.2 Vapor Doping Vapor doping offers a solvent-free alternative to conventional solution-based processing. This technique introduces dopants in the vapor phase, minimizing structural and morphological degradation. Figure 6a schematically illustrates the vapor doping process, which avoids pre-aggregation issues inherent in solution environments, thereby reducing phase separation and structural defects. As shown in Fig. 6b, Chabinyc et al. [84] compared the TE performance of solution-doped and vapor-doped films, finding that vapor doping achieved a over 50-fold enhancement in the  $\sigma$  of PBTTT over solution doping. Furthermore, annealing further significantly increased conductivity. Analysis of orientational correlation lengths demonstrated that vapordoped films exhibited enhanced molecular alignment of the PBTTT polymer chains. Complementary work by Cho's group [58] revealed that vapor doping enables simultaneous dopant incorporation in both amorphous and crystalline domains, while solution doping predominantly deposits dopants in amorphous regions.

For inorganic dopants, the vapor-phase infiltration (VPI) technique has been developed as an effective doping approach [72, 98] (Fig. 6c). Derived from atomic layer deposition, VPI enables self-limiting reactions between metallic precursors and oxidants [99, 100], thereby strengthening the bonding between inorganic dopants and organic matrices. Wang et al. [72] synthesized hybrid PBTTT-C<sub>14</sub> films via controlled in situ VPI using MoCl<sub>5</sub> and TiCl<sub>4</sub> as precursors. Owing to the strong Lewis acidity of MoCl<sub>5</sub>, which efficiently extracts electrons from the PBTTT backbone, the MoCl<sub>5</sub>-doped PBTTT films achieved a maximum conductivity of 67.1 S cm<sup>-1</sup> (Fig. 6d). Compared to conventional vapor doping methods, VPI method induces less perturbation to the chain conformation of polymer molecules.





82 Page 10 of 34 Nano-Micro Lett. (2026) 18:82

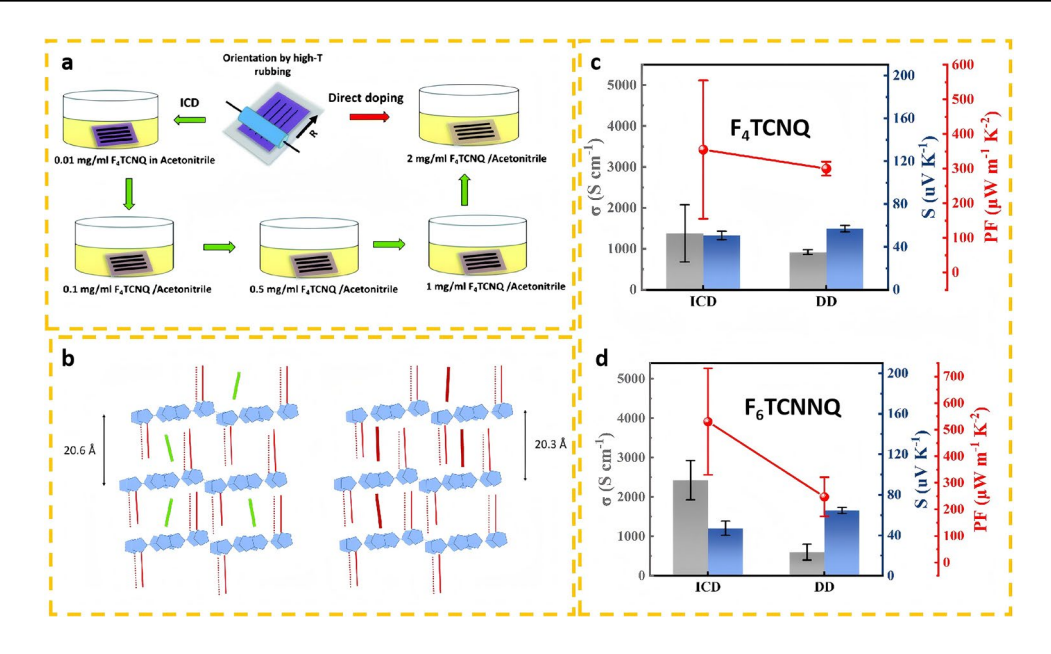


Fig. 5 Experimental process and data of the ICD method [96]. a Schematic of ICD method. b Schematic of the dopant intercalation of  $F_4$ TCNQ and  $F_6$ TCNNQ in the layers of alkyl side chains. c Comparison with ICD and DD doped with  $F_4$ TCNQ. d Comparison with ICD and DD doped with  $F_6$ TCNNQ

The orientational correlation length remains closer to its intrinsic state, and the doping depth offers greatly enhanced controllability.

3.1.2.3 Anion Exchange Doping Doping efficiency and charge carrier concentration are principally governed by the electrochemical redox potential difference between the  $\pi$ -conjugated polymer host and the dopant species [101]. For high-efficiency p-type doping, the electron affinity (EA) of the dopant must at least match the ionization potential (IP) of the polymer [102]. However, increasing the EA of dopants often compromises chemical stability, severely restricting viable dopant selection. To circumvent this limitation, Watanabe et al. [85] proposed an anion exchange doping approach (Fig. 7a), utilizing F<sub>4</sub>TCNQ as the p-type dopant and [EMIM][TFSI] as the charge transfer mediator. Figure 7a schematically illustrates the procedural workflow of anion exchange doping, which has two key features. First, the process is mediated by an IL solvent, where conventional small p-type dopant anions effectively and instantaneously exchange with a second anion provided by the IL. Introducing optimized ion salts into conventional binary donor-acceptor systems can overcome the oxidation-reduction potential limitations described by the Marcus theory, allowing for an anion exchange efficiency close to 100% and a  $\sigma$  of up to 620 S cm<sup>-1</sup>. Secondly, by adjusting the physicochemical properties of the additional anion, the thermal durability of the film can be further enhanced.

A mechanistic investigation of anion exchange doping was conducted by Sirringhaus et al. [93] to elucidate the fundamental processes governing this phenomenon. FeCl<sub>3</sub> was employed as the chemical dopant in conjunction with [BMP][TFSI] as a representative ion exchange electrolyte, enabling comprehensive analysis of the doping equilibrium and kinetic parameters in PBTTT films. Notably, the selection of acetonitrile as the processing solvent was found to substantially mitigate electrolyte association effects while simultaneously optimizing doping efficiency. By optimizing solvent selection and enhancing oxidizer strength, the thermodynamic constraints of traditional doping are overcome, leading to a further increase in the doping efficiency, hence, the  $\sigma$  of PBTTT can reach 1120 S cm<sup>-1</sup>.

Subsequently, Sirringhaus et al. investigated the influence of counterion size on TE performance [94]. They employed three anions of differing sizes: the bulky tris(trifluoromethylsulfonyl)methide anion (TFSM<sup>-</sup>), the moderately sized bis(trifluoromethylsulfonyl)imide anion (TFSI<sup>-</sup>), and the relatively small trifluoromethanesulfonate anion (TFO<sup>-</sup>). The TE performance results are presented in Fig. 7b. Crucially, these results revealed only a weak dependence of the TE performance on anion size. Instead,

Nano-Micro Lett. (2026) 18:82 Page 11 of 34 82

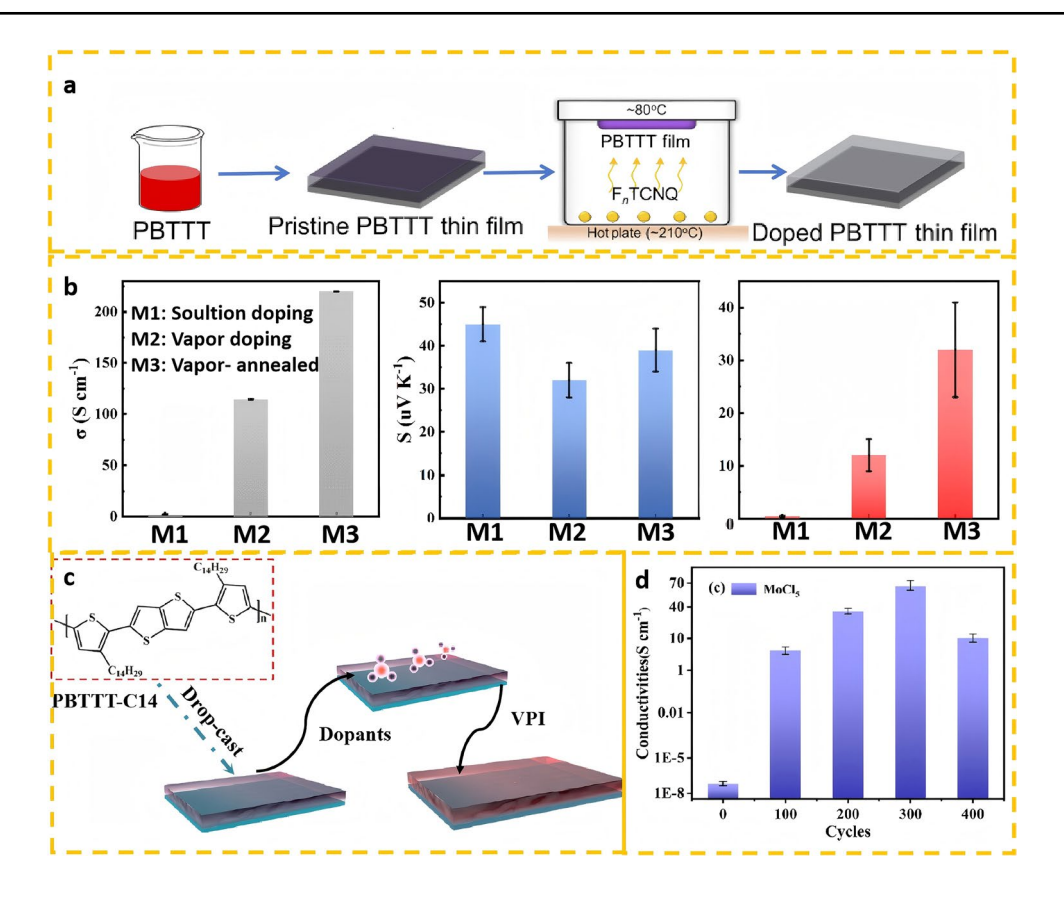


**Fig. 6** Schematic illustration of two typical vapor doping methods. **a** Schematic illustration of vapor doping process [84]. **b** A comparison of the effects of three treatment methods on TE performance, where M1 means solution doping, M2 denotes vapor doping and M3 refers to combination of vapor doping and annealed treatment [84]. **c** Schematic illustration of VIP. [72] and **d**  $\sigma$  of the PBTTT doped with MoCl<sub>5</sub> by VIP method [72]

the study identified that optimizing the spatial distribution of dopant ions within the film was key to achieving higher ZT.

#### 3.2 PBTTT Composites

In addition to doping, fabrication of composites is another means of enhancing TE performance. In composite materials, two or more different types of materials are combined to leverage the advantages of each material and compensate for their respective shortcomings, achieving a synergistic effect where 1+1>2 [103, 104].

Campoy-Quiles et al. [74] incorporated guest polymers into a PBTTT matrix with a mass fraction of 10%–15%, systematically investigating their influence on the TE properties of the host polymer. The researchers systematically screened nine guest materials (including P3HT, fullerene derivatives, and multiple donor polymers), establishing

a definitive composition-morphology-property relationship. As illustrated in Fig. 8a, incorporating 10 wt%–15 wt% P3HT into the host material PBTTT yields a remarkable five-fold enhancement of the PF compared to pristine PBTTT, achieving a ZT value of ~0.1. Further structural characterization revealed that annealing the 10 wt% P3HT blend at 180 °C spontaneously induces the formation of oriented ribbon-like nanostructures, analogous to the highly ordered phase observed in pure PBTTT annealed at a significantly higher temperature of 270 °C.

Carbon-based materials are dominant matrix candidates for flexible TE composites owing to their exceptional  $\sigma$  and mechanical robustness. Researchers have recently strategically incorporated PBTTT with carbon architectures, including carbon nanotubes (CNTs) [105, 106] and graphene [107]. However, limitations still persist in the PBTTT/CNT composite system. Cho et al. conducted a comparative investigation of PBTTT/CNT and





82 Page 12 of 34 Nano-Micro Lett. (2026) 18:82

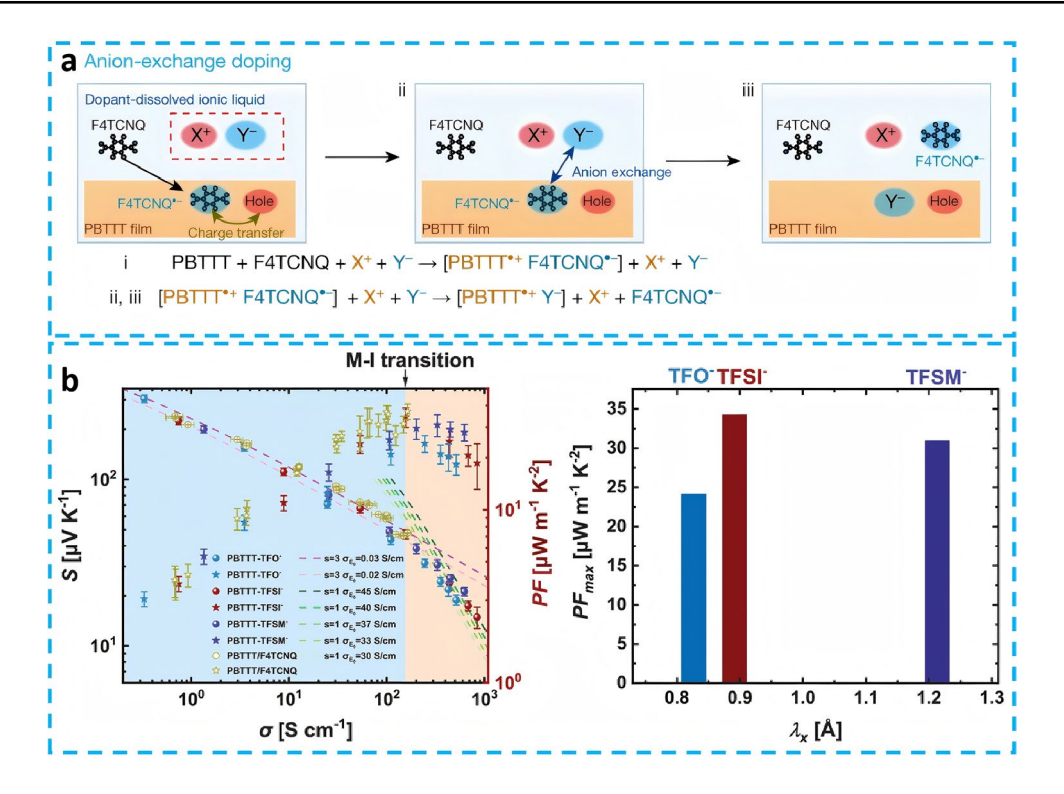


Fig. 7 Schematic illustration anion exchange doping. a Schematic illustration of anion exchange doping [85]. b In anion exchange doping, the effect of ion size on TE properties, using three different types of ions, i.e., TFO<sup>-</sup>, TFSI<sup>-</sup>, TFSM<sup>-</sup> [94]

indacenodithiophene-co-benzothiadiazole (IDTBT)/CNT composites using a combined experimental and molecular dynamics simulation, to elucidate interfacial charge transport mechanisms [106]. Analysis demonstrates that PBTTT tends to form thick aggregated shells on CNT surfaces (Fig. 8b), resulting in discontinuous charge transport pathways that hinder carrier hopping between adjacent CNTs, limiting  $\sigma$  to 169.9 S cm<sup>-1</sup>. In contrast, the IDTBT/CNT system achieves significantly higher  $\sigma$  (853.5 S cm<sup>-1</sup>) owing to continuous charge transport pathways.

To enhance the TE properties of PBTTT/CNT composites, structural modifications inspired by IDTBT can be implemented through backbone engineering, by introducing flexible copolymer units such as siloxane segments to reduce interchain stacking rigidity and designing branched side-chain architectures to improve molecular orientation freedom. In addition, surface modification for CNTs may achieve P3HT/PBTTT-like synergistic effects, strengthening  $\pi$ - $\pi$  interactions with CNTs and facilitating interfacial charge tunneling.

## 3.3 Aggregation State Controlling

The TE performance of PBTTT-based materials can also be significantly enhanced through the modulation of PBTTT chains' aggregation states, including molecular packing and crystallization dynamics. A critical advantage lies in PBTTT's liquid-crystalline phase, which inherently facilitates structural alignment and enables more refined control over its aggregation behavior during processing.

Well-ordered molecular arrangements optimize charge transport properties, leading to higher  $\sigma$  and S by reducing carrier scattering and enhancing delocalization within  $\pi$ -conjugated systems [82, 96]. Simultaneously, fine-tuning the crystalline morphology, such as lamellar stacking, grain boundary density, and degree of crystallinity, effectively suppresses phonon transport through selective scattering mechanisms, thereby minimizing  $\kappa$  while preserving high electronic mobility [108, 109]. The key tunable variables governing aggregation state include: solvent engineering, molecular structure design and thermal treatment [110].

Nano-Micro Lett. (2026) 18:82 Page 13 of 34 82

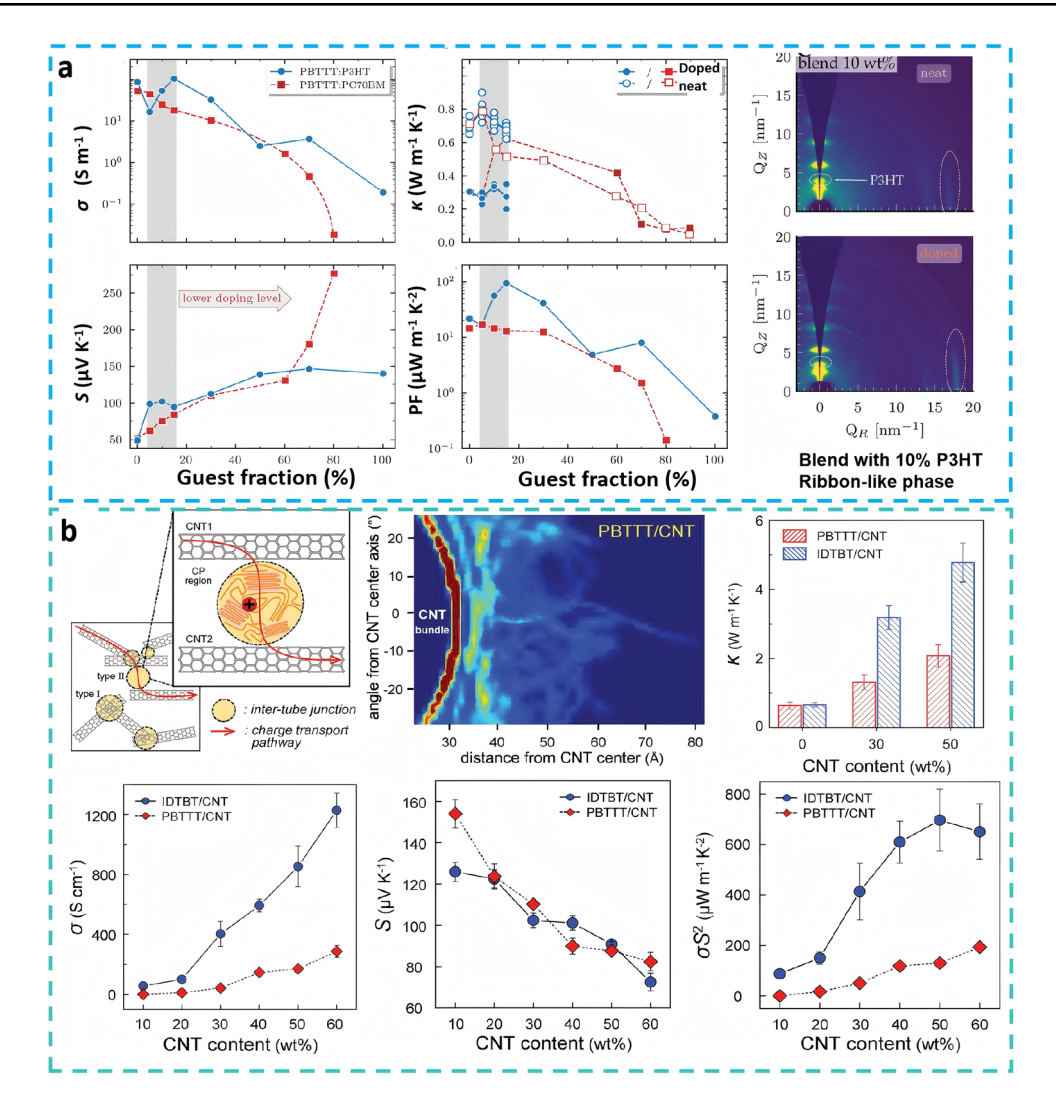


Fig. 8 Study on PBTTT-based composites. **a** TE properties for films of PBTTT with varied fractions of P3HT and PC70BM, and GIWAX images for the PBTTT blended with 10% P3HT annealed at 180 °C [74]. **b** Comparison of the TE properties between PBTTT/CNT composites and IDTBT/CNT composites [106]

#### 3.3.1 Solvent Engineering

Solution processability stands as a paramount advantage of conjugated polymers, enabling scalable fabrication of organic electronic devices through low-cost techniques [111–118]. Crucially, the solvent selection governs the crystallization kinetics and thermodynamic pathways during film formation, directly determining the TE performance of the resulting films. As evidenced by recent studies [112–114], the properties of solvents, boiling point, polarity, and solvent–solute interaction parameters, exert profound control over the crystallization behavior of PBTTT.

The study demonstrates that the boiling point of solvents plays a pivotal role in modulating both the morphology and film-forming mechanisms of PBTTT films via the FTM method [76]. For high-boiling-point solvents, the polymer solution spreads slowly across the aqueous substrate. During this static casting process, prolonged solvent evaporation allows thermodynamic self-assembly, resulting in isotropic films with edge-on molecular orientation. In contrast, low-boiling-point solvents initiate a dynamic casting regime: rapid solvent spreading, coupled with instantaneous evaporation, induces a transient lyotropic liquid-crystalline phase prior to solidification. In subsequent work [77], the





researchers further elucidated how solvent boiling temperature dictates PBTTT's crystallization behavior and charge carrier mobility. By comparing four solvents, i.e., chloroform (CF), trichloroethylene (TCE), chlorobenzene (CB), and 1,2-dichlorobenzene (DCB), they identified two distinct crystallization regimes: For low-boiling-point solvents (CF and TCE), rapid evaporation promotes kinetic trapping of PBTTT chains, yielding films with pronounced edge-on orientation; While for high-boiling-point solvents (CB and DCB), slow evaporation allows thermodynamic relaxation, leading to isotropic films. However, the correlation between mobility and crystallographic orientation follows a non-trivial trend (Fig. 9a). While low-boiling-point solvents yield better-aligned molecular packing, the resulting lower interchain coupling density leads to lower mobility. Conversely, high-boiling-point solvents produce isotropic films with reduced orientation but significantly enhanced  $\pi$ - $\pi$  stacking density through face-on dominated morphologies, ultimately delivering superior mobility.

82

In addition to the influence of solvent boiling points on the aggregation morphology of molecular chains, solvent polarity has been demonstrated to exert a marked impact on these structural features. As evidenced by the work of Yi et al. [115], systematic investigations into PBTTT aggregation states in toluene (Tol) and CB revealed contrasting mesoscale architectures governed by solvent-mediated thermodynamic and kinetic controls. Their analyses revealed a obvious dichotomy in aggregation behavior (Fig. 9b): In Tol, the low-polarity solvent facilitates rapid torsional relaxation of polymer backbones, enabling efficient  $\pi$ - $\pi$ stacking that drives the formation of anisotropic nanofibrils with aspect ratios > 3. In contrast, CB's higher polarity and steric hindrance from chlorine substituents disrupt ordered assembly, resulting in isotropic spherical aggregates with fractal dimensions < 2. This fundamental understanding of solvent-polymer dynamics provides critical guidelines for morphology control in solution-processed organic electronics. Gu and coworkers [118] further investigated the influence of solvent quality on PBTTT's aggregation behavior by analyzing CB and Tol systems through static light scattering experiments. By constructing Debye plots, they determined the second virial coefficients  $(A_2)$ , revealing that CB's positive A2 value classifies it as a good solvent that promotes polymer chain dissolution and dispersion, while Tol's negative A<sub>2</sub> value indicates poorer solvent quality that drives polymer chain aggregation. This comparative analysis demonstrates how solvent-mediated interactions critically regulate PBTTT's molecular assembly, providing an insight for controlling film morphology in organic electronic applications.

Moreover, solvent selection critically governs the thermodynamics of the annealing process, particularly in modulating nucleation kinetics and long-range ordering. Abdoul et al. [117] explored the synergistic effects of solvent selection (Tol, CB, and tetrahydrofuran (THF)) and thermal annealing on the crystalline morphology of PBTTT films. Their study revealed distinct solvent-dependent crystallization behaviors: when processed with CB, PBTTT formed a continuous and uniform nanofibrillar network upon annealing, facilitating efficient charge transport. In contrast, both Tol and THF induced the formation of a terraced liquid-crystalline phase above 120 °C annealing temperatures, as shown in Fig. 9c.

#### 3.3.2 Molecular Structure Design

3.3.2.1 Backbone Regulation The regulation of polymer backbone architecture has been predominantly directed toward molecular weight (MW) optimization to govern charge transport mechanisms [69, 119–122]. Higher-MW polymers inherently promote extended chain conformations, fostering enhanced interchain alignment and long-range crystalline order while intensifying π-orbital overlaps. Fan et al. [69] established a rigorous correlation between MW escalation in PBTTT-C<sub>14</sub> (MW: 11,867–175,199 g mol<sup>-1</sup>) and hierarchical structural ordering, observing a concurrent increase in  $\pi$ -π stacking and  $\sigma$  with rising MW, suggesting strengthened intermolecular interactions.

Advancing beyond uni-MW paradigms, Zhu et al. [122] developed a bimodal MW distribution strategy employing controlled blends of high-MW and low-MW PBTTT fractions (Fig. 10a). The low-MW polymer functioned as tiechains, bridging crystalline domains and improving intergrain charge transport while preserving TE performance. This approach yielded a high  $\sigma$  of 4,810 S cm<sup>-1</sup> and a PF of 173  $\mu$ W m<sup>-1</sup> K<sup>-2</sup> (Fig. 10b), without compromising the *S* or excessively increasing  $\kappa$ .

The blending of PBTTT chains with different MWs aligns conceptually with the host–guest strategy proposed by Campoy-Quiles et al. [74], aiming to establish a continuous network of interconnected polymer chains. While current studies utilize binary blending, future work could explore

Nano-Micro Lett. (2026) 18:82 Page 15 of 34 82

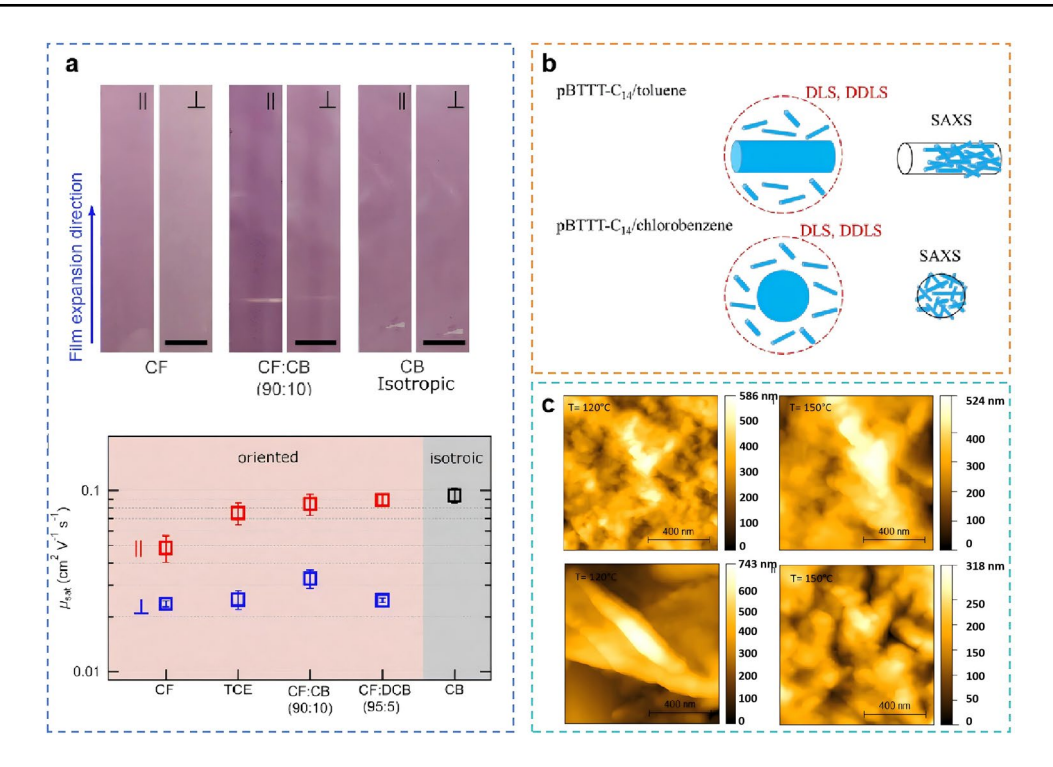


Fig. 9 Effect of solvents on the crystallization behavior of PBTTT. a Polarized photograph of the large-area films processed with different solvents and the corresponding carrier mobility [77]. b Schematic illustrations of a hierarchy of structural features of PBTTT-C<sub>14</sub> clusters incubated in two slightly different aromatic solvents [115]. c Solvent-dependent crystallization behaviors under 120 and 150 °C annealing temperature [117]

ternary blends (e.g., low/medium/high MW) to construct a more continuous tie-chain network, potentially breaking through existing electrical conductivity bottlenecks.

3.3.2.2 Side-Chain Engineering Beyond backbone modifications, side-chain engineering has emerged as a powerful approach to tailor polymer crystallization and electronic properties [65, 123–128]. Peng and coworkers [126] conducted systematic investigations of PBTTT derivatives functionalized with linear alkyl side chains ranging from hexyl ( $C_6$ ) to hexadecyl ( $C_{16}$ ). Through comprehensive characterization of crystalline structures and charge transport properties, they demonstrated that the combination of  $C_{14}$  side chains and high molecular weight synergistically promotes the formation of a highly ordered edge-on crystalline structure upon annealing at 180 °C (Fig. 11a), which exhibits optimal molecular alignment and achieves a remarkable hole mobility of 0.54 cm<sup>2</sup> V<sup>-1</sup> s<sup>-1</sup>.

Additionally, polar side chains can induce edge-on orientation of the polymer backbone. Polar ether-functionalized side chains (n-C<sub>7</sub>OC<sub>4</sub>) were incorporated in PBTTT (PBTTT-<sup>8</sup>O) by Durand et al. [127]. This modification significantly enhances the structural order of the PBTTT

backbone while improving thermal–mechanical properties, strengthening intrachain interactions. Comparative studies of F<sub>6</sub>TCNNQ-doped PBTTT-C<sub>12</sub> and PBTTT-<sup>8</sup>O reveal that the polar n-C<sub>7</sub>OC<sub>4</sub> side chains facilitate dopant dispersion, with F<sub>6</sub>TCNNQ molecules preferentially aligning within the disordered side-chain regions rather than disrupting backbone packing, as illustrated in Fig. 11b. These synergistic effects improved structural order, optimized dopant distribution, and enhanced charge transport, achieving a PF of 2.9 mW m<sup>-1</sup> K<sup>-2</sup>. Their further investigations into side-chain engineering [64] demonstrated that the position of oxygen atoms critically influences crystallinity: when placed farther from the backbone, oxygen disrupts chain packing less, promoting order by favoring a gauche conformation.

A comprehensive mechanistic study on the side-chain electronic modulation of PBTTT polymers conducted by Kurosawa et al. [65] reveals that alkoxy substituents induce a hypsochromic shift in HOMO energies. They demonstrated the strong electron-donating effect of alkoxy groups significantly upshifts the HOMO level, resulting in a lower ionization potential. The enhanced electron-donating character induces greater backbone planarity in





82 Page 16 of 34 Nano-Micro Lett. (2026) 18:82

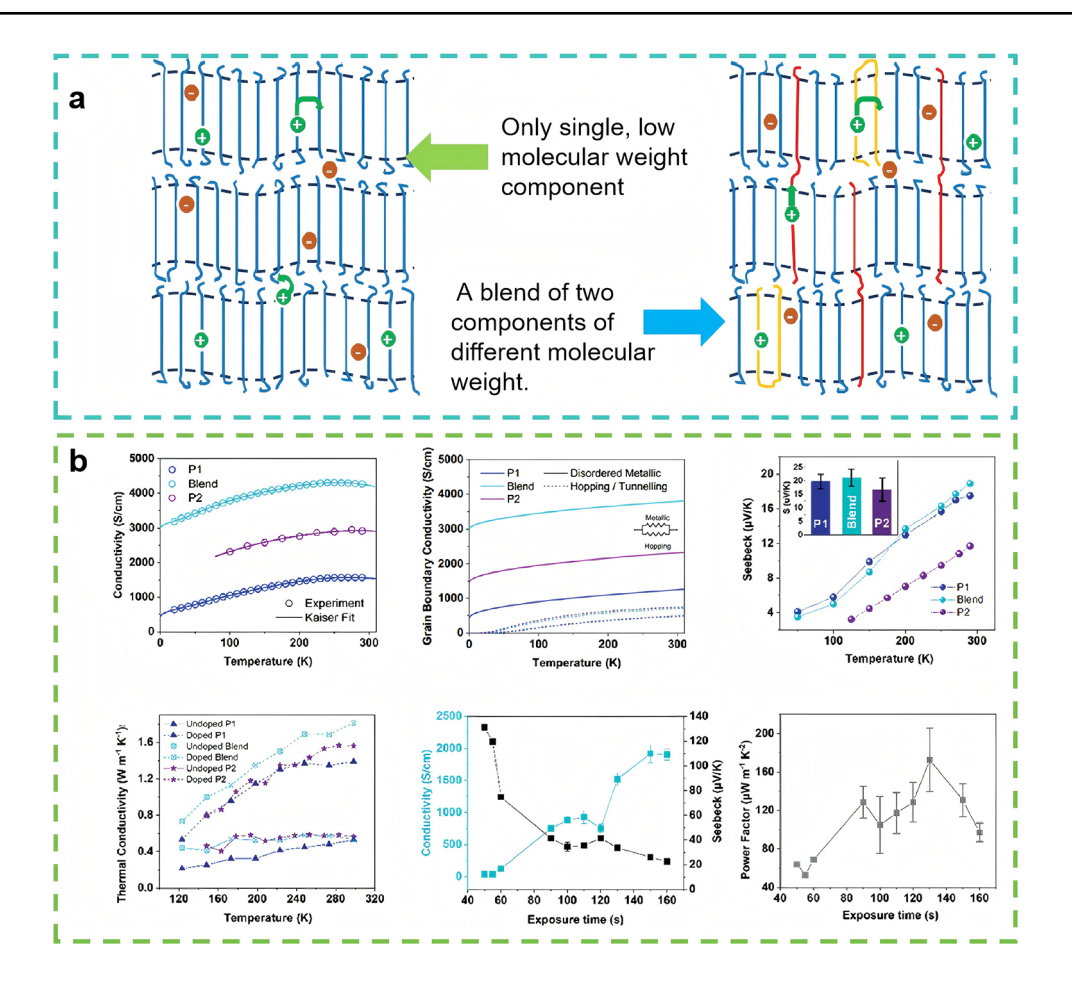


Fig. 10 Illustration of the influence of polymer backbone on crystallization. a Schematic of the aligned ribbon-phase with a single, low molecular weight component (left) and with a blend of two components of different molecular weight (right). b TE related properties of the blended-PBTTT, including conductivity, S and κ [122]

PBTTT, as evidenced by a higher torsional energy barrier relative to alkyl-substituted chains, which effectively reduces conformational disorder along the polymer backbone (Fig. 11c). These findings highlight the critical role of side-chain engineering in optimizing conjugated polymer performance.

Generally speaking, side-chain polarity, length, and branching profoundly impact backbone planarity, interchain  $\pi$ - $\pi$  stacking distance/donor-acceptor overlap, and energetic disorder. The future lies in integrated computational and AI-guided precision side-chain design, exemplified by exploring synergistic functional group combinations, implementing tailored molecular asymmetry, integrating ionic functionalities for mixed conduction or controlled doping, and harnessing programmable supramolecular interactions. Crucially, AI-enabled synergistic optimization with the conjugated backbone and dopants will be the decisive factor. Achieving

ultra-stable, high-performance organic TE materials through intelligent side-chain engineering presents a vital pathway toward energy harvesting and cooling applications.

#### 3.3.3 Melting-Induced Crystallization

PBTTT demonstrates a unique advantage over conventional conductive polymers due to the presence of liquid-crystalline phases [129, 130]. These liquid crystal phases, particularly the smectic mesophase, facilitate the long-range ordering of PBTTT molecular chains, thereby significantly enhancing its TE properties. While molten heating can induce the formation of these liquid-crystalline phases in PBTTT, achieving optimal alignment requires precise control over both temperature and cooling rate. Specifically, thermal processing conditions must be carefully tailored to harness the full potential

Nano-Micro Lett. (2026) 18:82 Page 17 of 34 82

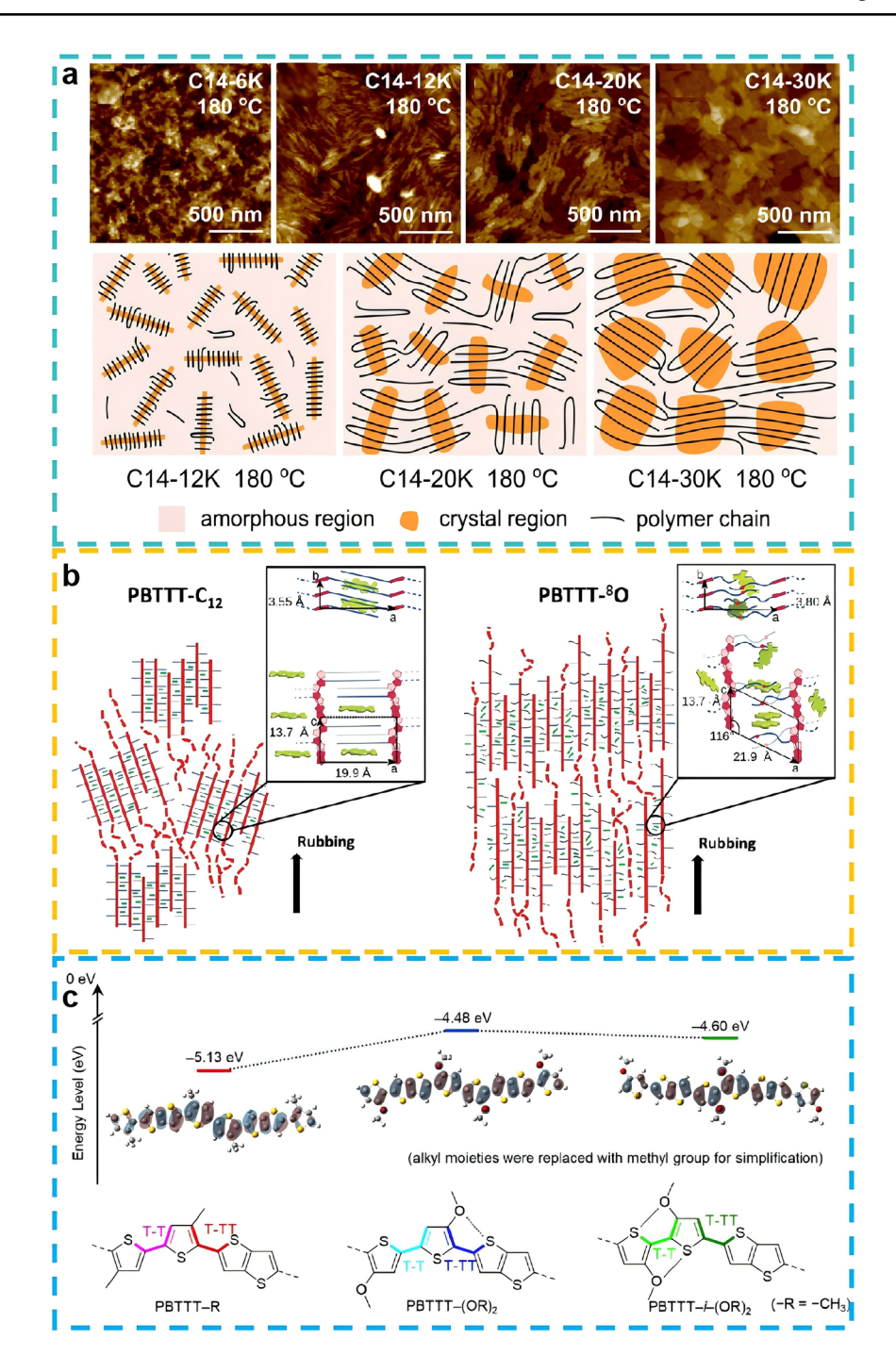


**Fig. 11** Illustration of the side-chain engineering. **a** AFM imaging of the modulation mechanism of MW and annealing temperature on the morphology and microstructure of PBTTT-C<sub>14</sub> [126]. **b** Schematic illustration of the mesoscale order induced by rubbing in PBTTT-C<sub>12</sub> (left) and PBTTT-<sup>8</sup>O (right) [127]. **c** Chemical structures and HOMO of PBTTT with alkyl side chains and alkoxyl side chains [65]

of PBTTT's liquid-crystalline behavior for improved charge transport performance.

Studies indicate that the cooling rate significantly influences the induction of two liquid crystal phases [129]. During the melt-cooling process, PBTTT can develop either a

nematic phase (LC I, Fig. 12a), characterized by long-range orientational order of molecular chains without positional regularity, or a smectic phase (LC II, Fig. 12b), in which molecules form well-defined layers with both orientational and in-plane positional order. The rapid cooling of the





liquid-crystalline polymer PBTTT effectively suppresses the nematic-to-smectic phase transition, significantly enhancing crystallinity and molecular ordering, leading to improved optoelectronic performance.

82

There remain divergent views regarding the evolution of PBTTT melt crystallization processes in current research. Zhou and coworkers [130] employed in situ Raman spectroscopy coupled with fast scanning calorimetry (FSC) to study the crystallization process of PBTTT. They found a threestage transformation process, as shown in Fig. 12c. At low temperatures (333 K), torsional dynamics of thienothiophene and thiophene rings generated a thermotropic mesophase with local order but long-range disorder; at intermediate temperatures (353–363 K), competition between backbone crystallization and mesophase preservation resulted in imperfect crystalline domains; while at elevated temperatures (413 K), enhanced backbone and side-chain mobility facilitated direct formation of highly crystalline structures. Martin et al. [131] believed that the conventionally labeled "annealing temperature" corresponds to a transition into a liquid-crystalline state rather than a crystalline phase. They found three distinct regimes (1) Below 120 °C, crystalline melting occurs, yielding either a glassy state or supercooled liquid; (2) Between 120 and 250 °C, a smectic liquid-crystalline phase with lamellar ordering emerges, albeit with limited long-range periodicity; and (3) Above 250 °C, the polymer transitions to a fully disordered isotropic liquid.

## 3.4 Recent-Developed Special Advances in PBTTT-Based TE Materials

Despite inherently lower TE performance compared to inorganic materials, state-of-the-art PBTTT-based TE materials have achieved comparable performance metrics through optimized doping techniques and crystallinity engineering. Crucially, these improvements preserve key organic advantages, including mechanical compliance and solution processability.

## 3.4.1 Doping Through Proton-Coupled Electron Transfer (PCET)

Yamashita et al. [132] proposed a proton-coupled electron transfer (PCET)-driven doping strategy to achieve atomic-level precision (±25 meV) in Fermi-level engineering for

PBTTT. While PCET mechanisms are ubiquitous in biological redox systems, their adaptation to organic semiconductors circumvents a critical limitation: Conventional doping inherently produces unstable dopant ions, whereas PCET synergizes non-ionic charge transfer with hydrophobic ion intercalation to decouple electrochemical activation from parasitic side reactions. As illustrated in Fig. 13a, the benzoquinone/hydroquinone (BO/HO) couple governs dual proton-electron transfers, with its pH-dependent redox potential self-regulated within the electrochemical stability window of aqueous environments, a design principle that inherently suppresses moisture-triggered degradation. Quantitative correlations between proton activity, optoelectronic properties, and energy-level realignment are systematically mapped in Fig. 13b. Higher proton activity (lower pH values) provides stronger oxidative power, driving the oxidation of more PBTTT molecules, thereby generating more hole carriers and significantly enhancing electrical conductivity. Meanwhile, the trend in the energy-level of PBTTT shifting with pH confirms that changes in proton activity directly determine the magnitude of the electrochemical driving force provided by the reaction. This enables precise and widerange control over the doping degree of the semiconductor, ultimately allowing accurate setting of its Fermi level.

Beyond proton activity, the oxidizer and anion selection significantly impact charge transport efficiency. As shown in Fig. 13c, they compared the effects of two oxidizers, 2,3-dichloro-5,6-dicyano-1,4-benzoquinone (DDQ) and DQ, and two anions, bis(nonafluorobutanesulfonyl)imide (NFSI<sup>-</sup>) and TFSI<sup>-</sup>. The strong oxidizer DDQ effectively oxidizes PBTTT, injecting a higher density of hole carriers. Concurrently, the NFSI<sup>-</sup> anion demonstrates exceptional charge transport properties. Consequently, the synergistic combination of the optimal oxidizer (DDQ) and the highest-conductivity anion (NFSI<sup>-</sup>) achieves a high electrical conductivity of 400 S cm<sup>-1</sup>.

## 3.4.2 Nanoconfined Electrochemical Ion Implantation (NEII) Doping

Previous studies primarily focused on precise control of doping effects, whereas Di et al. [133] extended this capability to the spatial domain. Drawing inspiration from ion implantation techniques in inorganic semiconductors, they developed the nanoconfined electrochemical ion

Nano-Micro Lett. (2026) 18:82 Page 19 of 34 82

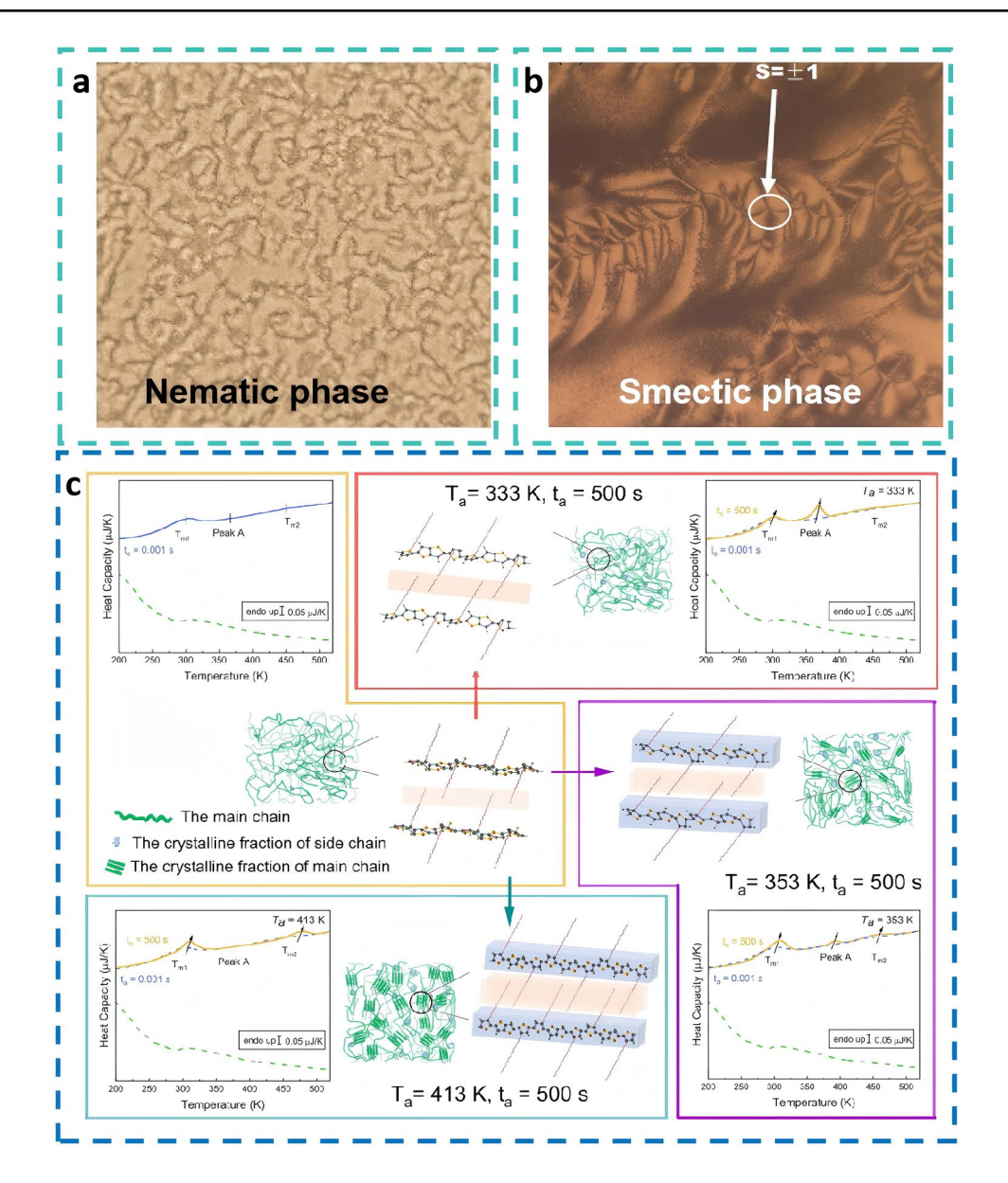


Fig. 12 Evolution of the liquid-crystalline phase in PBTTT. a Optical image of PBTTT film at the nematic phase [129]. b Optical image of PBTTT film at the smectic phase [129]. c Schematic illustration of the possible molecular ordering variety involved in the conformational evolution of PBTTT at different crystallization temperatures [130]

implantation (NEII) method, enabling sub-100-nm spatial precision doping. Figure 14a schematically illustrates the NEII mechanism: An AFM tip serves as a counterelectrode, while an electrolyte creates a fringing field that spatially constrains ion migration. This design effectively confines doping to the nanoscale. The electrolyte consists of polymethylmethacrylate (PMMA) blended with an ionic liquid, where the PMMA-to-ionic liquid ratio governs the glass transition temperature, a key parameter

determining the confinement characteristics. Figure 14b systematically analyzes the effects of both temperature and Tg on doping resolution. The results demonstrate an inverse relationship: increasing Tg enhances resolution, while higher temperatures degrade it. This tunable behavior provides a powerful means to optimize spatial control in organic semiconductor doping.

Considering that doping in crystalline regions primarily enhances  $\sigma$  while doping in amorphous regions boosts





82 Page 20 of 34 Nano-Micro Lett. (2026) 18:82

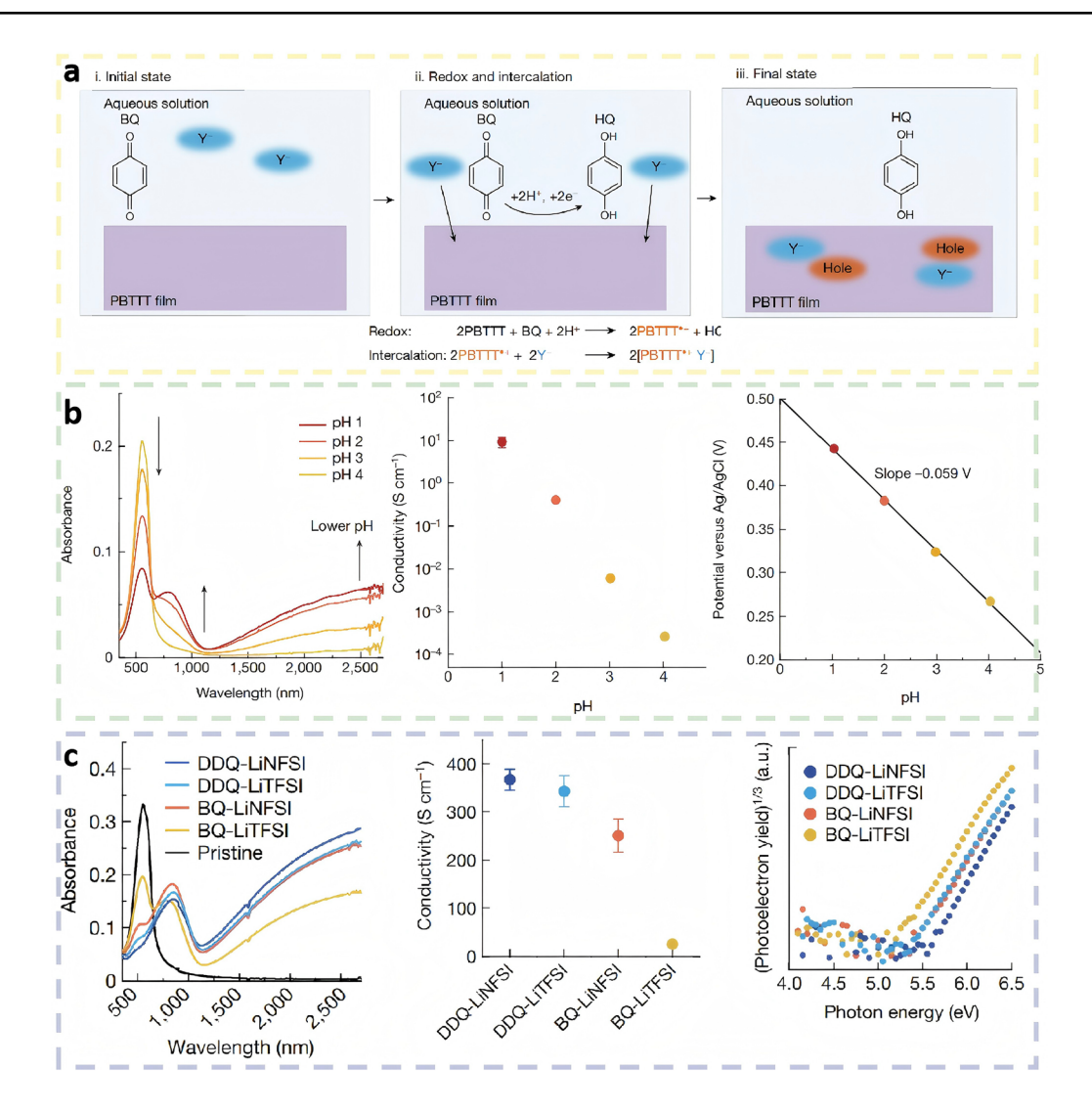


Fig. 13 Illustration of PCET method and its experimental data. a Schematics of the PCET doping process with the possible reaction equations. b Influence of the pH of the doping levels in PBTTT film on spectral absorbance,  $\sigma$ , and electrical potential. c Influence of the oxidants and dopant anions on spectral absorbance,  $\sigma$  and photoelectron yield spectroscopy [132]

the *S*, the integration of the NEII method with in situ molecular chain conformation characterization enables precise monitoring and manipulation of doping-induced structural reorganization in both ordered and disordered domains. This spatial-resolved control facilitates synergistic optimization of TE parameters, achieving maximization of PF.

#### 3.4.3 Multi-heterojunctioned PBTTT Composite

Most current strategies for the enhancement of TE properties focus overwhelmingly on electrical optimization,

while systematic approaches for governing  $\kappa$  remain underdeveloped. Zhao and coworkers proposed an innovative methodology targeting  $\kappa$  suppression to optimize TE performance [59]. They designed a periodic two-dimensional heterojunction architecture, which enables precise manipulation of phonon scattering pathways, achieving a suppression of  $\kappa$  while maintaining excellent charge transport. As illustrated in Fig. 15a, the heterojunctions were constructed using selenium-substituted diketopyrrolopyrrole polymer (PDPPSe-12) and PBTTT. A four-armed azide-based crosslinker was employed to achieve nanoscale layer-bylayer stacking via ultraviolet light crosslinking. Chemical doping was implemented through immersion in FeCl<sub>3</sub>/ Nano-Micro Lett. (2026) 18:82 Page 21 of 34 82

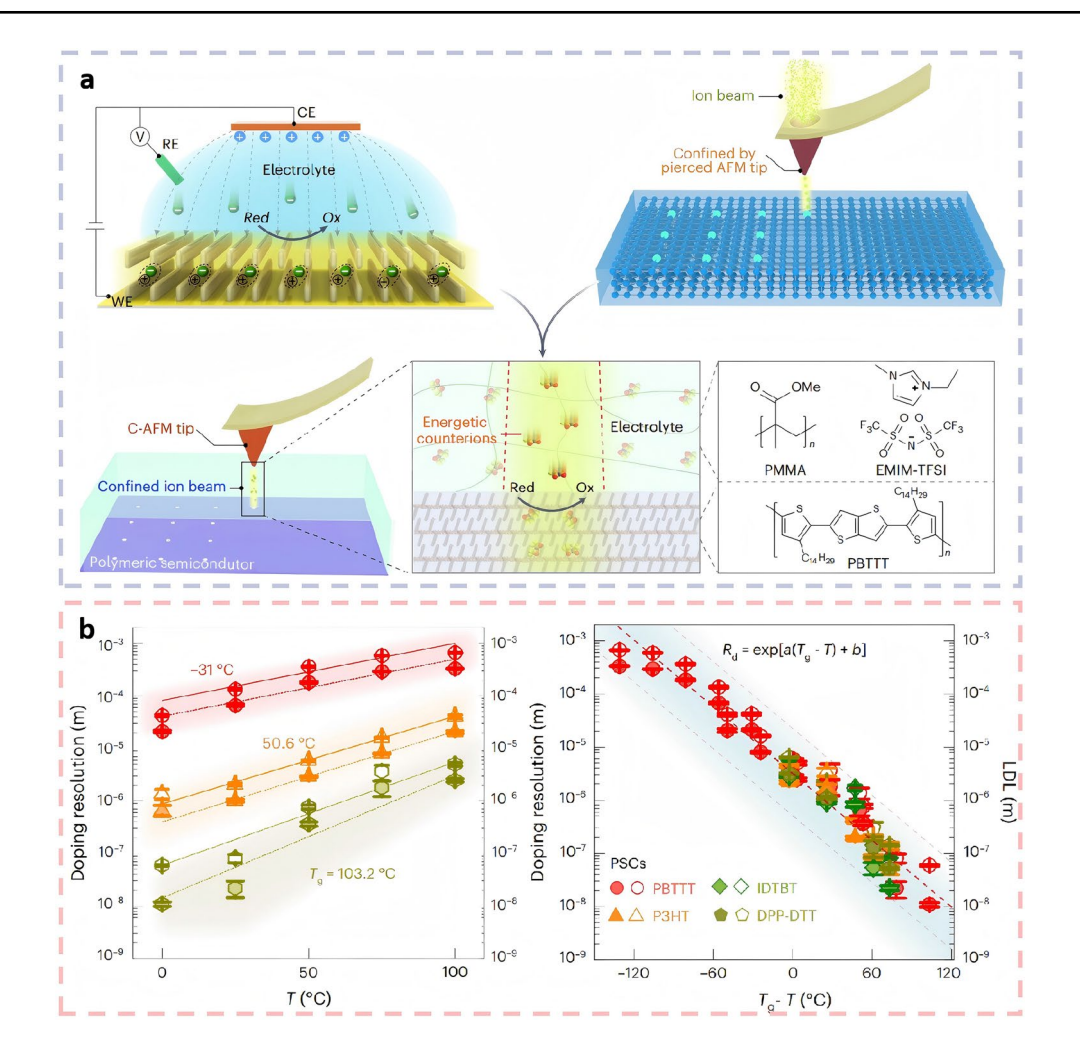


Fig. 14 Illustration of NEII doping and its experimental data. a Schematics of the NEII doping process, in which the counterions is confined by both the conductive AFM tip and the reshaped fringing field in the electrolyte. b T- and Tg-dependent doping resolution [133]

nitromethane solution. This fabrication protocol exhibited excellent structural consistency, enabling large-area coating  $(35\times21~{\rm cm}^2)$  with a uniform thickness of  $16.2\pm2.6~{\rm nm}$ . The structure incorporates interfaces scaled to the phonon mean free path length, enabling strong interfacial phonon scattering while maintaining efficient charge transport channels. The out-of-plane  $\kappa_{\perp}$  reduced to 0.06 W m<sup>-1</sup> K<sup>-1</sup> (Fig. 15b), showing a substantial 55% and 76% reduction compared to pristine PBTTT and PDPPSe-12 films, respectively. The measurement of  $\kappa_{\perp}$  is mutually validated through  $3\omega$ -Scanning thermal microscopy  $(3\omega$ -SThM) and the suspended microdevice method, ensuring result reliability.

Remarkably, the heterojunction simultaneously enhances both the S and  $\sigma$  relative to single-component films. This

synergistic improvement yields an exceptional PF of 628  $\mu$ W m<sup>-1</sup> K<sup>-2</sup> at 368 K, culminating in a record *ZT* value of 1.28. Two mechanisms underlie this performance breakthrough: (1) Doping effects that optimize carrier concentration; (2) quasi-2D charge transport in the heterostructure, where interfacial charge transfer increases electronic entropy. The flexible TE generator (TEG) architectured with the heterojunction thin-film modules (Fig. 15c) demonstrated an output power of 522 nW under an applied temperature gradient of 38 K. The TEG exhibited robust mechanical stability (>95% conductivity retention after 100,000 bending cycles) and generated 3.3 mV open-circuit voltage on human skin. The optimized power density (1.12  $\mu$ W cm<sup>-2</sup> K<sup>-2</sup>) positions this architecture as a scalable,





82 Page 22 of 34 Nano-Micro Lett. (2026) 18:82

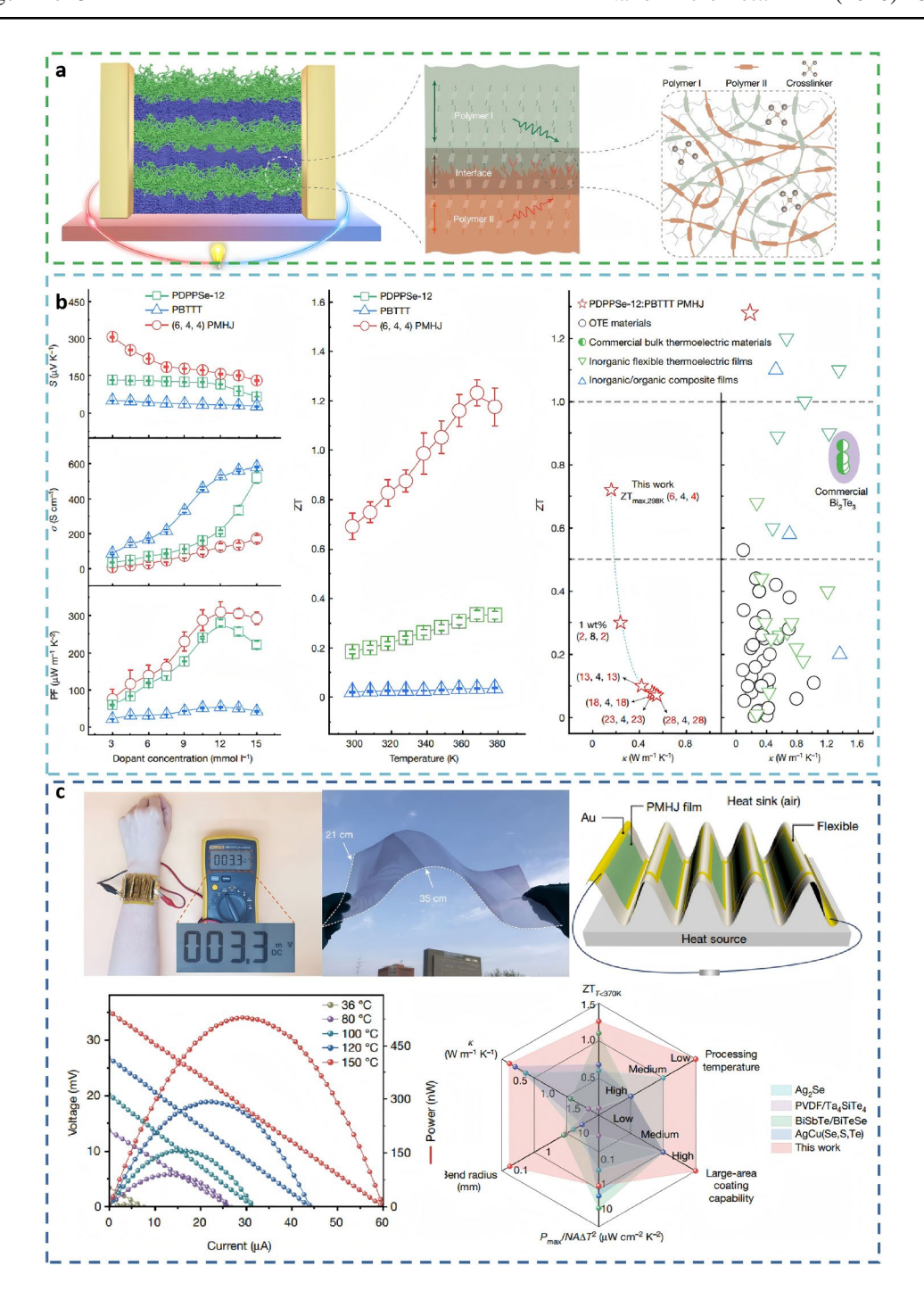


Fig. 15 Illustration of the structure and experimental data for the multi-heterojunctioned PBTTT composite. a Schematic of the structure. b Variation of TE performance with temperature and dopant concentration, including  $\sigma$ , S, PF,  $\kappa$ , and ZT. c Schematic illustration of the flexible integrated TEG and power output measurement [59]

cost-effective platform for powering IoT devices and flexible electronics from low-grade waste heat.

### 3.5 Brief Summary

Doping remains the most prevalent method for optimizing TE performance. It enhances conductivity by modulating carrier concentration, yet faces challenges such as Nano-Micro Lett. (2026) 18:82 Page 23 of 34 82

environmental instability. While anion doping improves stability, bulky anions increase  $\pi$ – $\pi$  stacking distance and reduce conductivity. Current doping strategies are advancing toward refinement, with progress in spatial and energy-level precision control. The PCET doping method achieves precise energy-level manipulation but is restricted by pH responsiveness, effective only in strongly acidic conditions, while rendering it unsuitable for biological environments or mildly acidic scenarios. NEII technology addresses core challenges in polymeric nanodoping through glassy electrolyte confinement effects, though it requires overcoming the "high-resolution vs. high-conductivity" trade-off dilemma.

For composites, PBTTT/CNT blends suffer from poor dispersion and phase separation, while PBTTT combined with other conductive polymers yields limited TE improvement. Composites leveraging hetero-interface phonon selective scattering can suppress lattice thermal conductivity while preserving high electrical conductivity. However, complex fabrication processes, interface thickness sensitivity, and ultrathin-film limitations result in low power output.

Regarding aggregation state control, current research primarily emphasizes crystallization mechanisms but inadequately explores harnessing crystalline control to enhance TE performance. Given that crystallinity optimization, side-chain engineering, and strategic doping collectively govern charge transport and phonon scattering dynamics, future investigations should pursue synergistic integration of these factors.

The advantages and disadvantages of the three approaches are presented in Table 2. Overall, each method possesses its own merits and limitations, while combining multiple techniques enables synergistic enhancement by leveraging their complementary effects. TE performance optimization strategies are evolving toward an integrated approach that strategically combines crystallization control, side-chain engineering, and advanced doping techniques, harnessing their complementary advantages while mitigating individual limitations. Future endeavors will leverage machine learning and other advanced techniques to conduct multivariate parameter optimization, achieving fine-tuned and customized control over TE performance.

## **4 TE Properties**

In the previous section, we summarized specific methods to improve TE performance. In this section, we have compiled and summarized the reported TE of PBTTT. Table 3 gives the TE performances of PBTTT-related materials reported in literature. Below, we summarize the critical advancements in each category.

#### 4.1 Electrical Conductivity

The  $\sigma$  is determined by both the charge carrier concentration and the carrier mobility, as expressed by the equation:

$$\sigma = ne\mu. \tag{2}$$

Here, n represents the carrier concentration, e is the elementary charge, and  $\mu$  is the carrier mobility. By employing doping strategies [134–136], electron acceptors or donors can be introduced into conjugated polymers to increase carrier concentration. In addition, chain conformation modulations [137, 138] can influence charge transport properties and enhancing mobility. It has been proved that gas-phase doping can increase the PF by an order of magnitude compared to solution doping [90]. In recent years, the development of anion exchange doping has further improved doping efficiency [69, 94]. The optimization strategies discussed in the third section primarily focus on enhancing  $\sigma$ . According to Table 3, it can be seen that the  $\sigma$  of PBTTT has increased by three to four orders of magnitude from its initial value of less than 5 S cm<sup>-1</sup> [71, 127].

#### 4.2 Seebeck Coefficient

According to the Mott formula [139] in degenerately doped semiconductors, the expression for *S* is:

$$S = \frac{\pi^2 k_B^2}{3e} T \left\{ \frac{\mathrm{d}n(E)}{n\mathrm{d}E} + \frac{\mathrm{d}\mu(E)}{\mu\mathrm{d}E} \right\}_{E=E_c}.$$
 (3)

E represents the carrier energy, and dn(E)/dE is equivalent to the slope of the carrier Density of States (DOS). As shown in Eqs. (2) and (3), carrier concentration and mobility are positively correlated with  $\sigma$  but negatively correlated with S. Consequently, there exists a trade-off between optimizing S and  $\sigma$ .





Fable Strate Mech

82

ole 2 Adva	ole 2 Advantages and disadvantages of doping, composites and aggregation state control	regation state control		
ategy	Doping	Composites	Aggregation State Control	
chanism	Redox reactions or ion exchange to adjust carrier concentration	Hybrids with carbon materials (CNTs, graphene) or polymers	Solvent/thermal tuning of crystallinity and chain alignment	
vantages	<ul> <li>(1) Directly controlling carrier concentration enables precisely engineering significantly enhanced electrical conductivity;</li> <li>(2) Ensuring compatibility with existing device fabrication processes facilitates high-volume manufacturing</li> </ul>	<ul> <li>(1) Hetero-interfaces selectively scatter phonons while preserving charge carriers, holding the promise for decoupling thermal and electronic transport</li> <li>(2) Enabling the integration of multiple functionalities</li> </ul>	<ul> <li>(1) Conductivity enhanced through carrier transport trajectory optimization, without disrupting the crystal lattice structure</li> <li>(2) Suppression of lattice thermal conductivity via nanoboundary design;</li> <li>(3) Solution processability with simplified fabrication</li> </ul>	
advantages	<ul> <li>advantages (1) Dopants exhibit susceptibility to deactivation and chemical/environmental sensitivity;</li> <li>(2) High doping levels readily compromise lattice integrity and disrupt crystalline structure;</li> <li>(3) While doping boosts σ, it concurrently depresses the <i>S</i> and frequently elevates κ</li> </ul>	(1) PBTTT demonstrates poor compatibility with CNTs, leading to unfavorable phase separation (2) Blending with P3HT offers only moderate performance improvement, thus necessitating complementary doping strategies (3) The fabrication of heterojunction structures is complex. The thin film is very thin, resulting in low output power	(1) Slow crystallization kinetics and poor repeatability (2) Sensitivity to solvent polarity; (3) Deficient TE enhancement necessitates compensation through strategic doping	
				_

Some studies are dedicated to decoupling S and  $\sigma$ . Katz et al. [136] found that using nitrosonium tetrafluoroborate (NOBF<sub>4</sub>), a kind of strong polar dopant, can decouple S and  $\sigma$ . Their results demonstrate that while either S or  $\sigma$  is increased, the other parameter can be stabilized or slightly increased through offsetting energy levels and improving intermolecular interactions. Considering that PBTTT is thermoplastic, Brinkmann et al. [64, 82, 127] improved the long-range order of PBTTT polymer chains through high-T rubbing, stretching, and annealing. The structural optimization effectively modulates charge transport pathways while minimizing the adverse impact on thermopower, thereby providing another viable pathway for partial S- $\sigma$  decoupling.

In conductive polymers like PEDOT, the energy filtering strategy has been widely explored to decouple the S and  $\sigma$  [140, 141]. By introducing controlled energy barriers, low-energy charge carriers can be selectively filtered out, thereby increasing the average carrier energy. However, in PBTTT-based systems, comparable studies remain scarce. Despite its promising TE properties, the application of energy filtering and its impact on S- $\sigma$  decoupling, has not yet been systematically investigated, presenting an important avenue for future research.

#### 4.3 Thermal Conductivity

The total  $\kappa$  consists of two components: electronic thermal conductivity ( $\kappa_e$ ) and phononic thermal conductivity ( $\kappa_p$ ),

$$\kappa = \kappa_{\rm e} + \kappa_{\rm p}.\tag{4}$$

For crystalline materials,  $\kappa_{\rm e}$  and  $\sigma$  obey the Wiedemann-Franz law,

$$\kappa_{\rm e} = LT\sigma.$$
(5)

Here, L represents the Lorenz number. For TE materials, high  $\sigma$  but low  $\kappa$  is desired. Therefore, to improve TE conversion efficiency, we aim to minimize  $\kappa_p$  while preserving  $\kappa_e$ .

Currently, experimental data on the  $\kappa$  of PBTTT remains limited, primarily due to the significantly greater technical challenges associated with thermal measurements compared to electrical characterization methods. The most common measurement for  $\kappa$  is 3- $\omega$  method [142, 144], which determines in-plane  $\kappa$  by applying a sinusoidal alternating current  $(1-\omega)$ to a metal microheater, inducing axial temperature oscillations via Joule heating. The 1- $\omega$  input signal generates a 3- $\omega$  voltage

 Table 3
 TE performances of PBTTT-related materials reported in literature

Type of PBTTT	Treatment	ZT	PF, $\mu W m^{-1} K^{-2}$	$\sigma$ , $S \text{ cm}^{-1}$	$S$ , $\mu V K^{-1}$	$\kappa$ , W m <sup>-1</sup> K <sup>-1</sup>	Refs	Year
PBTTT-C <sub>14</sub>	Drop casting; Doped with NOPF <sub>6</sub> ; Annealed		0.98	53.8	13.5		[134]	2012
PBTTT-C <sub>14</sub>	Solution casting; Solution doped with F <sub>4</sub> TCNQ		$1.3 \pm 0.4$	$3.51 \pm 0.05$	$60\pm9$		[71]	2014
PBTTT-C <sub>14</sub>	Vapor deposition of FTS		$25 \pm 8$	$466 \pm 0.1$	$23 \pm 4$		Ditto	
PBTTT-C <sub>12</sub>	Drop casting; Doped with TFSI <sup>-</sup>		3.71	220	13		[135]	2014
PBTTT-C <sub>14</sub>	Vapor doping with F <sub>4</sub> TCNQ; Annealed		32±9	$220.00 \pm 0.02$	$39 \pm 5$		[84]	2017
PBTTT-C <sub>14</sub>	Vapor doping with F <sub>2</sub> TCNQ; Annealed		$70 \pm 20$	$36\pm3$	$140 \pm 20$		Ditto	
PBTTT-C <sub>12</sub>	High-T rubbing; Subsequent solution doping with FeCl <sub>3</sub>		1944±626 // (in-plane)	$(2.2 \pm 0.5) \times 10^5$ //	9.4±0.5 //		[75]	2019
			0.47	$2100 \pm 300$	$1.5\pm0.5$			
			$\perp$ (out-of-plane)	Τ	Τ			
$\begin{array}{c} \text{PBTTT-C}_{12} \\ \text{PBTTTS-C}_{12} \text{ blend} \end{array}$	Drop casting; Solution doping with NOBF <sub>4</sub>		1.2	510	4.85		[136]	2019
PBTTT-C <sub>7</sub> OC <sub>4</sub>	F <sub>6</sub> TCNNQ doping; High-T rubbing up to 240 °C		2900	$5 \times 10^4$	24.1		[127]	2022
PBTTT- <sup>8</sup> O	Doped with F <sub>6</sub> TCNNQ; High-T rubbing		256	3250	4.2		[82]	2022
PBTTT-C <sub>14</sub> P3HT blend	F <sub>4</sub> TCNQ	0.1	97	101	98	0.3	[74]	2022
PBTTT-C <sub>14</sub>	Ion Exchange Doped; Anion: TFSI-		$34.2 \pm 4.3$	70	71		[ <mark>94</mark> ]	2023
PBTTT-C <sub>14</sub>	Ion Exchange Doped; Anion: TFSM <sup>-</sup>		$30.9 \pm 4.5$	100	30.9		Ditto	
$PBTTT-C_{14}$	Ion Exchange Doped; Anion: TFO-		$24.2 \pm 2.7$	105	48		Ditto	
PBTTT- <sup>11</sup> O	Doped with F <sub>6</sub> TCNNQ and aligned by high-T rubbing		496.2	59	29		[64]	2024
PBTTT- <sup>8</sup> O	Ditto		2928.2	$5 \times 10^4$	24.2		Ditto	
PBTTT- <sup>5</sup> O	Ditto		1324.8	23,000	24		Ditto	
PBTTT- <sup>3</sup> O	Ditto		729	10,000	27		Ditto	
PBTTT-C <sub>14</sub>	Two step doping: Solution doping with F <sub>4</sub> TCNQ, followed by ion exchange doping		$26.97 \pm 1.05$	941.1	$16.93 \pm 0.4$		[69]	2024
PBTTT-C <sub>12</sub>	Ion-exchange doping; Blending of high and low molecular weight chains		173	4810	18.9		[122]	2024
PBTTT-C <sub>14</sub>	Doped with BCF		230	140	128		[73]	2024
PgBTTT	Doped with BCF		$223 \pm 4$	$2180 \pm 360$	$32 \pm 1.3$		[87]	2024
PBTTT-C <sub>12</sub>	Modifying the substrate with self- assembled monolayers		30.7	320	31		[137]	
PBTTT - $C_{14}$	PDPPSe-12 and PBTTT heterojunction structure	1.28	628 (at 368 K)	196	179	0.18	[59]	2024
PBTTT - $C_{14}$	Supramolecular nucleating agent (PDA) doping strategy		176	1894	30.4		[138]	2025





signal, and combined with the one-dimensional heat diffusion equation, the material's in-plane  $\kappa$  can be derived.

82

The fundamental challenge in  $\kappa$  regulation resides in the inherent coupling between thermal and electrical properties. Taking inspiration from inorganic TE research, researchers engineered interfaces at specific scales by leveraging the disparity in mean free paths between electrons and phonons [59], achieving selective enhancement of phonon scattering while preserving electronic transport. Furthermore, a systematic investigation led by Campoy-Quiles et al. [109] on 17 conjugated polymers with varying chain conformations revealed that molecular chain conformation critically affects the  $\kappa$ - $\sigma$  decoupling. They found that for structures with long-range order,  $\kappa$  and  $\sigma$  are positively correlated and cannot be decoupled. For amorphous and short-range ordered conjugated polymers, effective decoupling of charge and thermal transport can be achieved. Their research findings provide a research direction for enhancing TE performance by controlling  $\kappa$ . In addition, introducing interfaces in composite systems can also effectively reduce  $\kappa$ .

## 5 Summary and Outlook

## 5.1 Summary of Research Status

Positioned as a uniquely processable material in OTE field, PBTTT has demonstrated dual-solvent/melt-processing adaptability, thus occupying a pivotal position among conducting polymers for energy harvesting applications. This review systematically examines the cutting-edge progress in PBTTT-based TE materials, with particular emphasis on synthesis strategies, performance enhancement mechanisms, and emerging technological frontiers.

Regarding synthesis protocols, PBTTT and its derivatives primarily employ the Stille cross-coupling methodology for backbone construction. Subsequent solution-processing techniques (e.g., spin coating, blade coating, floating film transfer) dominate composite fabrication, endowing PBTTT architectures with tailorable nanomorphology and device compatibility.

Critical advancements in optimizing TE performance primarily focus on three strategic approaches: (1) Charge carrier engineering via doping methodologies, including solution-phase doping, vapor-phase infiltration, and anion exchange doping; (2) Composite structure regulation, where synergistic combinations of material systems increasingly outperform single-component modifications; (3) Aggregation state control, which can be achieved through solvent optimization, thermal processing, and molecular chain design. Significantly, singular enhancement strategies have become inadequate to address contemporary performance requirements. To maximize TE property enhancements, state-of-the-art research emphasizes the synergistic integration of multiple approaches. For instance, combining doping with high-T rubbing, backbone design with anion exchange, and solid-state diffusion with anion exchange.

Furthermore, we have summarized the existing literature on the TE data of PBTTT-related materials. The most extensively studied TE properties include S and  $\sigma$ . There exists a trade-off relationship between S and  $\sigma$ , and researchers are dedicated to decoupling the mutual influence between the two, aiming to maximize the PF. Over the course of a decade, the PF of PBTTT has increased from initially being less than 1  $\mu$ W m<sup>-1</sup> K<sup>-2</sup> by two to three orders of magnitude.

Finally, we present the latest research developments regarding PBTTT in the field of TE. PCET doping not only enhances the stability of dopants in the environment but also allows for precise Fermi level tuning with an accuracy of 25 meV. NEII doping enables spatially high-resolution doping, with resolutions as low as 100 nm. Multi-heterojunctioned PBTTT composites simultaneously regulate  $\sigma$ , S, and  $\kappa$ , achieving a remarkable ZT value of up to 1.28 at 368 K.

## **5.2** Challenges and Opportunities

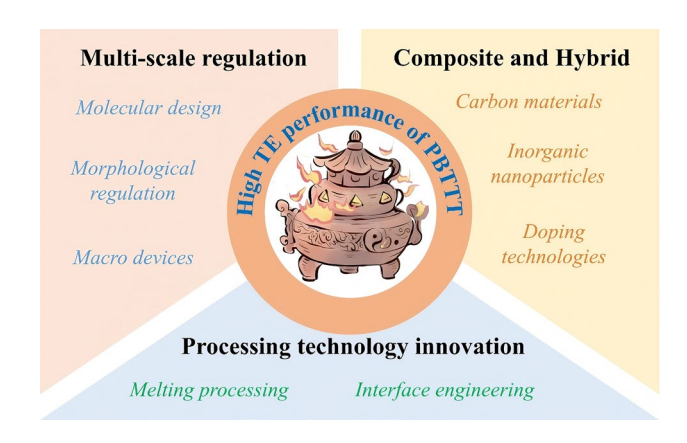
Although significant progress has been made in improving the TE performance of PBTTT through various optimization strategies in recent years, further research has unveiled emerging opportunities and challenges. As illustrated in Fig. 16, these include but are not limited to the following three key aspects:

(1) Multiscale regulation. Multiscale regulation enables synergistic optimization of TE performance, encompassing molecular-scale design, micro/nanomorphological control, and macroscopic device engineering. At the molecular level, backbone optimization and side-chain engineering of PBTTT can be employed to modify conjugation lengths and band structures through chemical modifications, thereby altering charge transport mechanisms. The micro/

Nano-Micro Lett. (2026) 18:82 Page 27 of 34 82

nanostructural level focuses on regulating the liquid-crystal-line phase ordering of PBTTT. Precise control over crystal-linity and phase separation is critical for enhancing carrier mobility while suppressing  $\kappa$ . At the macroscopic device level, despite PBTTT has achieved a notable ZT value of 1.28, its power output still remains limited to 522 nW. The low output power primarily stems from its intrinsic resistance and the high contact resistance during device assembly. Therefore, strengthening innovation at the macro device level, such as jointless p-n and device integration design, can improve overall TE performance. This discrepancy highlights the need for holistic optimization across all length scales to bridge the gap between material-level properties and device performance, and significant to improve energy conversion efficiency.

(2) Composite and hybrid strategies. Many prominent studies have demonstrated the significant impact of composite hybridization approaches on enhancing the TE performance of PBTTT, including those carbon material incorporation, inorganic nanoparticle dispersion, and doping. Carbon-based hybridization facilitates the formation of continuous conductive pathways within the polymer matrix, dramatically improving charge carrier mobility. Graphene and carbon nanotubes have proven particularly effective in establishing percolation networks that enhance  $\sigma$  while maintaining favorable S. Inorganic nanoparticle integration leverages interfacial effects to promote energy filtering mechanisms. In addition, new doping methods also have a surprising effect on improving TE performance. This selective scattering process



 $\begin{tabular}{ll} Fig.~16 & Potential strategies for achieving high TE performance with PBTTT \\ \end{tabular}$ 

preferentially transmits high-energy charge carriers, thereby simultaneously increasing the S and preserving  $\sigma$ , which is a crucial advantage for achieving high ZT values. However, the research on the  $\kappa$  of PBTTT is currently insufficient. The  $\kappa$  of conjugated polymers encompasses lattice thermal conduction and electronic thermal conduction. In metallic materials, the  $\kappa_{\rm e}$  and  $\sigma$  directly adhere to the Wiedemann-Franz Law. However, in conjugated polymers, whether this law holds true remains an opening question. Therefore, only by investing more in fundamental understanding of the mechanisms governing  $\kappa$  in PBTTT can we effectively reconcile the interrelationships among these three critical parameters to ultimately maximize the ZT value. This requires accurate thermal measurements, an area where traditional techniques like timedomain thermoreflectance (TDTR) and the 3- $\omega$  method face limitations due complex sample preparations, high instrumentation costs, substrate interference effects and so on. To overcome these constraints in organic TE film characterization, Wang et al. [145] recently proposed a laser spot periodic heating technique based on sub-region phase fitting. This approach minimizes sample preparation requirements and enables rapid determination of thermal conductivity, promising significant advances for future thermal measurements of PBTTT and other organic TE films.

(3) Innovative material processing techniques. Currently, the advantages of melt processibility for PBTTT have not been fully utilized. While most conjugated polymers are typically processed using solution-based methods to produce TE films, PBTTT can be processed not only via solution methods but also through melt-processing techniques such as injection molding, extrusion, rolling, melt spinning, and others. However, there is currently limited research on using melt-processing methods to fabricate PBTTT-based TE materials. Only a small amount of literature reports on the use of high-T rubbing to process PBTTT films, aiming to improve molecular chain orientation and enhance TE performance. The impact of meltprocessing methods on its TE properties requires further investigation. Additionally, interfacial engineering during processing, such as modulating energy levels, microstructures, and phonon/electron transport, should be considered to optimize TE performance.

Anyway, of the individual strategies, improvements are often limited to specific aspects of performance. For





instance, doping generally yields the most immediate boost in  $\sigma$ , whereas composite engineering can tackle  $\kappa$  via phonon scattering, and morphology control often helps balance  $\sigma$  and S. Extensive evidence indicates that the synergistic integration of methods (such as first orienting polymer chains before doping, or designing new main chains that better accommodate dopants) is the key to achieving recordbreaking performance. Only through close coordination among diverse strategies can the advancement of PBTTT applications be accelerated.

**Acknowledgements** We thank the financial support by Guangdong Basic and Applied Basic Research Foundation (2025A1515012415), National Natural Science Foundation of China (52242305), and the Stable Support Project of Shenzhen (Project No. 20231122125728001).

Author Contributions Zhenqiang Ye involved in conceptualization, investigation, and writing. Mingdong Zhang was responsible for literature research on "Doping" section. Junyang Deng was responsible for literature research on "PBTTT Composites" section. Lirong Liang and Chunyu Du contributed to literature screening on "Aggregation State Control" section. Guangming Chen was responsible for conceptualization, review, funding acquisition, and supervision.

#### **Declarations**

82

**Conflict of interest** The authors declare no conflict of interest. They have no known competing financial interests or personal relationships that could have influenced the work reported in this paper. Guangming Chen, an editorial board member for Nano-Micro Letters, was not involved in the editorial review or decision to publish this article.

Open Access This article is licensed under a Creative Commons Attribution 4.0 International License, which permits use, sharing, adaptation, distribution and reproduction in any medium or format, as long as you give appropriate credit to the original author(s) and the source, provide a link to the Creative Commons licence, and indicate if changes were made. The images or other third party material in this article are included in the article's Creative Commons licence, unless indicated otherwise in a credit line to the material. If material is not included in the article's Creative Commons licence and your intended use is not permitted by statutory regulation or exceeds the permitted use, you will need to obtain permission directly from the copyright holder. To view a copy of this licence, visit http://creativecommons.org/licenses/by/4.0/.

#### References

1. T.M. Gür, Review of electrical energy storage technologies, materials and systems: challenges and prospects for

- large-scale grid storage. Energy Environ. Sci. **11**(10), 2696–2767 (2018). https://doi.org/10.1039/C8EE01419A
- Q. Yan, M.G. Kanatzidis, High-performance thermoelectrics and challenges for practical devices. Nat. Mater. 21(5), 503– 513 (2022). https://doi.org/10.1038/s41563-021-01109-w
- 3. Q. Tang, B. Jiang, K. Wang, W. Wang, B. Jia et al., Highentropy thermoelectric materials. Joule **8**(6), 1641–1666 (2024). https://doi.org/10.1016/j.joule.2024.04.012
- Y. Lu, Y. Zhou, W. Wang, M. Hu, X. Huang et al., Staggered-layer-boosted flexible Bi<sub>2</sub>Te<sub>3</sub> films with high thermoelectric performance. Nat. Nanotechnol. 18(11), 1281–1288 (2023). https://doi.org/10.1038/s41565-023-01457-5
- 5. Y. Xiao, L.-D. Zhao, Charge and phonon transport in PbTe-based thermoelectric materials. NPJ Quantum Mater. **3**, 55 (2018). https://doi.org/10.1038/s41535-018-0127-y
- K. Peng, X. Lu, H. Zhan, S. Hui, X. Tang et al., Broad temperature plateau for high ZTs in heavily doped p-type SnSe single crystals. Energy Environ. Sci. 9(2), 454–460 (2016). https://doi.org/10.1039/C5EE03366G
- O. Caballero-Calero, J.R. Ares, M. Martín-González, Environmentally friendly thermoelectric materials: high performance from inorganic components with low toxicity and abundance in the Earth. Adv. Sustain. Syst. 5(11), 2100095 (2021). https://doi.org/10.1002/adsu.202100095
- Z. Soleimani, S. Zoras, B. Ceranic, S. Shahzad, Y. Cui, The cradle to gate life-cycle assessment of thermoelectric materials: a comparison of inorganic, organic and hybrid types. Sustain. Energy Technol. Assess. 44, 101073 (2021). https:// doi.org/10.1016/j.seta.2021.101073
- B. Russ, A. Glaudell, J.J. Urban, M.L. Chabinyc, R.A. Segalman, Organic thermoelectric materials for energy harvesting and temperature control. Nat. Rev. Mater. 1(10), 16050 (2016). https://doi.org/10.1038/natrevmats.2016.50
- L. Deng, Y. Liu, Y. Zhang, S. Wang, P. Gao, Organic thermoelectric materials: niche harvester of thermal energy. Adv. Funct. Mater. 33(3), 2210770 (2023). https://doi.org/10.1002/adfm.202210770
- 11. X. Fan, W. Nie, H. Tsai, N. Wang, H. Huang et al., PEDOT: PSS for flexible and stretchable electronics: modifications, strategies, and applications. Adv. Sci. 6(19), 1900813 (2019). https://doi.org/10.1002/advs.201900813
- H. He, J. Ouyang, Enhancements in the mechanical stretchability and thermoelectric properties of PEDOT: PSS for flexible electronics applications. Acc. Mater. Res. 1(2), 146–157 (2020). https://doi.org/10.1021/accountsmr.0c000 21
- K.M. Reza, A. Gurung, B. Bahrami, S. Mabrouk, H. Elbohy et al., Tailored PEDOT: PSS hole transport layer for higher performance in perovskite solar cells: enhancement of electrical and optical properties with improved morphology. J. Energy Chem. 44, 41–50 (2020). https://doi.org/10.1016/j. jechem.2019.09.014
- B. Chen, M. Wu, S. Fang, Y. Cao, L. Pei et al., Liquid metaltailored PEDOT: PSS for noncontact flexible electronics with high spatial resolution. ACS Nano 16(11), 19305–19318 (2022). https://doi.org/10.1021/acsnano.2c08760

Nano-Micro Lett. (2026) 18:82 Page 29 of 34 82

15. W. Jeong, G. Gwon, J.-H. Ha, D. Kim, K.-J. Eom et al., Enhancing the conductivity of PEDOT: PSS films for biomedical applications *via* hydrothermal treatment. Biosens. Bioelectron. **171**, 112717 (2021). https://doi.org/10.1016/j.bios.2020.112717

- I. Paulraj, T.F. Liang, T.S. Yang, C.H. Wang, J.L. Chen et al., High performance of post-treated PEDOT: PSS thin films for thermoelectric power generation applications. ACS Appl. Mater. Interfaces 13(36), 42977–42990 (2021). https://doi. org/10.1021/acsami.1c13968
- M. Mooney, A. Nyayachavadi, S. Rondeau-Gagné, Ecofriendly semiconducting polymers: from greener synthesis to greener processability. J. Mater. Chem. C 8(42), 14645– 14664 (2020). https://doi.org/10.1039/d0tc04085a
- 18. C. Dai, B. Liu, Conjugated polymers for visible-light-driven photocatalysis. Energy Environ. Sci. **13**(1), 24–52 (2020). https://doi.org/10.1039/c9ee01935a
- C. Chen, Z. Liu, L. Guo, B. Huo, Q. Sun et al., High spatiotemporal resolution biomimetic thermoreceptors realizing by jointless p-n integration thermoelectric composites. Adv. Funct. Mater. 34(49), 2411490 (2024). https://doi.org/10.1002/adfm.202411490
- C. Du, M. Cao, G. Li, Y. Hu, Y. Zhang et al., Toward precision recognition of complex hand motions: wearable thermoelectrics by synergistic 2D nanostructure confinement and controlled reduction. Adv. Funct. Mater. 32(36), 2206083 (2022). https://doi.org/10.1002/adfm.202206083
- Z. Ding, C. Du, W. Long, C.-F. Cao, L. Liang et al., Thermoelectrics and thermocells for fire warning applications. Sci. Bull. 68(24), 3261–3277 (2023). https://doi.org/10.1016/j.scib.2023.08.057
- 22. Z. Ding, G. Li, Y. Wang, C. Du, Z. Ye et al., Ultrafast response and threshold adjustable intelligent thermoelectric systems for next-generation self-powered remote IoT fire warning. Nano-Micro Lett. **16**(1), 242 (2024). https://doi.org/10.1007/s40820-024-01453-x
- 23. G. Li, Y. Hu, J. Chen, L. Liang, Z. Liu et al., Thermoelectric and photoelectric dual modulated sensors for human Internet of Things application in accurate fire recognition and warning. Adv. Funct. Mater. 33(41), 2303861 (2023). https://doi.org/10.1002/adfm.202303861
- 24. Q. Sun, C. Du, G. Chen, Thermoelectric materials and applications in buildings. Prog. Mater. Sci. **149**, 101402 (2025). https://doi.org/10.1016/j.pmatsci.2024.101402
- 25. Z. Liu, C. Chen, J. Liu, Q. Sun, B. Huo et al., All-day solar power generation enabled by photo/thermoelectric conversion and thermal energy storage. Sci. China Chem. **68**(5), 2035–2043 (2025). https://doi.org/10.1007/s11426-024-2336-1
- H. Lv, L. Liang, Y. Zhang, L. Deng, Z. Chen et al., A flexible spring-shaped architecture with optimized thermal design for wearable thermoelectric energy harvesting. Nano Energy 88, 106260 (2021). https://doi.org/10.1016/j.nanoen.2021. 106260
- 27. H. Li, Z. Ding, Q. Zhou, J. Chen, Z. Liu et al., Harness high-temperature thermal energy *via* elastic thermoelectric

- aerogels. Nano-Micro Lett. **16**(1), 151 (2024). https://doi.org/10.1007/s40820-024-01370-z
- X. Lu, Z. Mo, Z. Liu, Y. Hu, C. Du et al., Robust, efficient, and recoverable thermocells with zwitterion-boosted hydrogel electrolytes for energy-autonomous and wearable sensing. Angew. Chem. Int. Ed. 63(29), e202405357 (2024). https://doi.org/10.1002/anie.202405357
- S. Wang, G. Zuo, J. Kim, H. Sirringhaus, Progress of conjugated polymers as emerging thermoelectric materials. Prog. Polym. Sci. 129, 101548 (2022). https://doi.org/10.1016/j.progpolymsci.2022.101548
- Z. Qiu, B.A.G. Hammer, K. Müllen, Conjugated polymers– problems and promises. Prog. Polym. Sci. 100, 101179 (2020). https://doi.org/10.1016/j.progpolymsci.2019.101179
- A. Pron, P. Rannou, Processible conjugated polymers: from organic semiconductors to organic metals and superconductors. Prog. Polym. Sci. 27(1), 135–190 (2002). https://doi.org/ 10.1016/S0079-6700(01)00043-0
- J.F. Ponder Jr., S.A. Gregory, A. Atassi, A.K. Menon, A.W. Lang et al., Significant enhancement of the electrical conductivity of conjugated polymers by post-processing side chain removal. J. Am. Chem. Soc. 144(3), 1351–1360 (2022). https://doi.org/10.1021/jacs.1c11558
- 33. A. Moliton, R.C. Hiorns, Review of electronic and optical properties of semiconducting π-conjugated polymers: applications in optoelectronics. Polym. Int. **53**(10), 1397–1412 (2004). https://doi.org/10.1002/pi.1587
- 34. C.K. Chiang, C.R. Fincher, Y.W. Park, A.J. Heeger, H. Shirakawa et al., Electrical conductivity in doped polyacetylene. Phys. Rev. Lett. **39**(17), 1098–1101 (1977). https://doi.org/10.1103/physrevlett.39.1098
- 35. C.I. Simionescu, V. Percec, Progress in polyacetylene chemistry. Prog. Polym. Sci. **8**(1–2), 133–214 (1982). https://doi.org/10.1016/0079-6700(82)90009-0
- 36. S. Deng, C. Dong, J. Liu, B. Meng, J. Hu et al., An n-type polythiophene derivative with excellent thermoelectric performance. Angew. Chem. Int. Ed. **62**(18), e202216049 (2023). https://doi.org/10.1002/anie.202216049
- P.-S. Lin, S. Inagaki, J.-H. Liu, M.-C. Chen, T. Higashihara et al., The role of branched alkylthio side chain on dispersion and thermoelectric properties of regioregular polythiophene/carbon nanotubes nanocomposites. Chem. Eng. J. 458, 141366 (2023). https://doi.org/10.1016/j.cej. 2023.141366
- S. Liu, H. Li, P. Li, Y. Liu, C. He, Recent advances in polyaniline-based thermoelectric composites. CCS Chem. 3(10), 2547–2560 (2021). https://doi.org/10.31635/ccschem.021. 202101066
- H. Li, Y. Liu, P. Li, S. Liu, F. Du et al., Enhanced thermoelectric performance of carbon nanotubes/polyaniline composites by multiple interface engineering. ACS Appl. Mater. Interfaces 13(5), 6650–6658 (2021). https://doi.org/10.1021/ acsami.0c20931
- 40. A. Debnath, K. Deb, K. Sarkar, B. Saha, Low interfacial energy barrier and improved thermoelectric performance





- in Te-incorporated polypyrrole. J. Phys. Chem. C **125**(1), 168–177 (2021). https://doi.org/10.1021/acs.jpcc.0c09100
- M. Almasoudi, M.S. Zoromba, M.H. Abdel-Aziz, M. Bassyouni, A. Alshahrie et al., Optimization preparation of one-dimensional polypyrrole nanotubes for enhanced thermoelectric performance. Polymer 228, 123950 (2021). https://doi.org/10.1016/j.polymer.2021.123950

82

- 42. L. Wu, H. Li, H. Chai, Q. Xu, Y. Chen et al., Anion-dependent molecular doping and charge transport in ferric salt-doped P3HT for thermoelectric application. ACS Appl. Electron. Mater. **3**(3), 1252–1259 (2021). https://doi.org/10.1021/acsae lm.0c01067
- 43. V. Untilova, T. Biskup, L. Biniek, V. Vijayakumar, M. Brinkmann, Control of chain alignment and crystallization helps enhance charge conductivities and thermoelectric power factors in sequentially doped P3HT: F4TCNQ films. Macromolecules 53(7), 2441–2453 (2020). https://doi.org/10.1021/acs.macromol.9b02389
- M.N. Gueye, A. Carella, J. Faure-Vincent, R. Demadrille, J.-P. Simonato, Progress in understanding structure and transport properties of PEDOT-based materials: a critical review. Prog. Mater. Sci. 108, 100616 (2020). https://doi.org/10. 1016/j.pmatsci.2019.100616
- L. Liu, J. Chen, L. Liang, L. Deng, G. Chen, A PEDOT: PSS thermoelectric fiber generator. Nano Energy 102, 107678 (2022). https://doi.org/10.1016/j.nanoen.2022.107678
- Y. Li, Y. Pang, L. Wang, Q. Li, B. Liu et al., Boosting the performance of PEDOT: PSS based electronics *via* ionic liquids. Adv. Mater. 36(13), 2310973 (2024). https://doi.org/10.1002/adma.202310973
- N. Wen, Z. Fan, S. Yang, Y. Zhao, T. Cong et al., Highly conductive, ultra-flexible and continuously processable PEDOT:
   PSS fibers with high thermoelectric properties for wearable energy harvesting. Nano Energy 78, 105361 (2020). https://doi.org/10.1016/j.nanoen.2020.105361
- 48. I. McCulloch, M. Heeney, C. Bailey, K. Genevicius, I. Mac-Donald et al., Liquid-crystalline semiconducting polymers with high charge-carrier mobility. Nat. Mater. **5**(4), 328–333 (2006). https://doi.org/10.1038/nmat1612
- J.G. Sutjianto, S.H. Yoo, C.R. Westerman, T.N. Jackson, J.J. Wilker et al., Blends of conjugated and adhesive polymers for sticky organic thin-film transistors. Adv. Electron. Mater. 9(12), 2300422 (2023). https://doi.org/10.1002/aelm.20230 0422
- P.-A. Chen, J. Guo, H. Wei, J. Xia, C. Chen et al., Achieving unipolar organic transistors for complementary circuits by selective usage of doped organic semiconductor film electrodes. Adv. Funct. Mater. 35(3), 2413880 (2025). https:// doi.org/10.1002/adfm.202413880
- J. Vanderspikken, Q. Liu, Z. Liu, T. Vandermeeren, T. Cardeynaels et al., Tuning electronic and morphological properties for high-performance wavelength-selective organic near-infrared cavity photodetectors. Adv. Funct. Mater. 32(9), 2108146 (2022). https://doi.org/10.1002/adfm.202108146
- 52. S. Gupta, B.N. Pal, R. Prakash, Improved ammonia sensitivity and broadband photodetection by using PBTTT-C14/

- WS<sub>2</sub>-QDs nano-heterojunction based thin film transistor. Sens. Actuators B Chem. **414**, 135872 (2024). https://doi.org/10.1016/j.snb.2024.135872
- L.-H. Li, O.Y. Kontsevoi, S.H. Rhim, A.J. Freeman, Structural, electronic, and linear optical properties of organic photovoltaic PBTTT-C14 crystal. J. Chem. Phys. 138(16), 164503 (2013). https://doi.org/10.1063/1.4802033
- D.W. Gehrig, I.A. Howard, S. Sweetnam, T.M. Burke, M.D. McGehee et al., The impact of donor–acceptor phase separation on the charge carrier dynamics in pBTTT: PCBM photovoltaic blends. Macromol. Rapid Commun. 36(11), 1054–1060 (2015). https://doi.org/10.1002/marc.201500112
- M.U. Chaudhry, K. Muhieddine, R. Wawrzinek, J. Sobus, K. Tandy et al., Organic light-emitting transistors: advances and perspectives. Adv. Funct. Mater. 30(20), 1905282 (2020). https://doi.org/10.1002/adfm.201905282
- F.-C. Wu, P.-R. Li, B.-R. Lin, R.-J. Wu, H.-L. Cheng et al., Ultraviolet light-activated charge modulation heterojunction for versatile organic thin film transistors. ACS Appl. Mater. Interfaces 13(38), 45822–45832 (2021). https://doi.org/10. 1021/acsami.1c12390
- S.A. Gregory, A. Atassi, J.F. Ponder Jr., G. Freychet, G.M. Su et al., Quantifying charge carrier localization in PBTTT using thermoelectric and spectroscopic techniques. J. Phys. Chem. C 127(25), 12206–12217 (2023). https://doi.org/10.1021/acs.jpcc.3c01152
- J. Min, D. Kim, S.G. Han, C. Park, H. Lim et al., Positioninduced efficient doping for highly doped organic thermoelectric materials. Adv. Electron. Mater. 8(3), 2101142 (2022). https://doi.org/10.1002/aelm.202101142
- 59. D. Wang, J. Ding, Y. Ma, C. Xu, Z. Li et al., Multi-heterojunctioned plastics with high thermoelectric figure of merit. Nature **632**(8025), 528–535 (2024). https://doi.org/10.1038/s41586-024-07724-2
- V. Raja, Z. Hu, G. Chen, Progress in poly(2, 5-bis(3-alkylthiophen-2-yl)thieno [3, 2-b] thiophene) composites for thermoelectric application. Compos. Commun. 27, 100886 (2021). https://doi.org/10.1016/j.coco.2021.100886
- 61. S. Tierney, M. Heeney, I. McCulloch, Microwave-assisted synthesis of polythiophenes *via* the Stille coupling. Synth. Met. **148**(2), 195–198 (2005). https://doi.org/10.1016/j.synthmet.2004.09.015
- 62. Z. Bao, W. Chan, L. Yu, Synthesis of conjugated polymer by the stille coupling reaction. Chem. Mater. **5**(1), 2–3 (1993). https://doi.org/10.1021/cm00025a001
- 63. J.-P. Lère-Porte, J.J.E. Moreau, C. Torreilles, Highly conjugated poly(thiophene)s—synthesis of regioregular 3-alkylthiophene polymers and 3-alkylthiophene/thiophene copolymers. Eur. J. Org. Chem. **2001**(7), 1249–1258 (2001). https://doi.org/10.1002/1099-0690(200104) 2001:7%3c1249::AID-EJOC1249%3e3.0.CO;2-F
- P. Durand, H. Zeng, B. Jismy, O. Boyron, B. Heinrich et al., Controlling conjugated polymer morphology by precise oxygen position in single-ether side chains. Mater. Horiz. 11(19), 4737–4746 (2024). https://doi.org/10.1039/D4MH0 0492B

Nano-Micro Lett. (2026) 18:82 Page 31 of 34 82

- 65. T. Kurosawa, Y. Yamashita, Y. Kobayashi, C.P. Yu, S. Kumagai et al., Employment of alkoxy sidechains in semicrystalline semiconducting polymers for ambient-stable p-doped conjugated polymers. Macromolecules **57**(1), 328–338 (2024). https://doi.org/10.1021/acs.macromol.3c00211
- P.-J. Yu, Y.-C. Lin, C.-Y. Lin, W.-C. Chen, Enhanced mobility preservation of polythiophenes in stretched states utilizing thienyl-ester conjugated side chain. Polymer 264, 125575 (2023). https://doi.org/10.1016/j.polymer.2022.125575
- 67. J. Vanderspikken, Z. Liu, X. Wu, O. Beckers, S. Moro et al., On the importance of chemical precision in organic electronics: fullerene intercalation in perfectly alternating conjugated polymers. Adv. Funct. Mater. **33**(52), 2309403 (2023). https://doi.org/10.1002/adfm.202309403
- 68. Z. Liu, J. Vanderspikken, P. Mantegazza, S. Moro, M. Hamid et al., Removing homocoupling defects in alkoxy/alkyl-PBTTT enhances polymer: fullerene co-crystal formation and stability. Adv. Funct. Mater. (2024). https://doi.org/10. 1002/adfm.202413647
- Y. Fan, J. Liu, P.-A. Chen, D. Xia, J. Wang et al., Doping regulation of highly conductive PBTTT films. Cell Rep. Phys. Sci. 5(9), 102197 (2024). https://doi.org/10.1016/j.xcrp.2024. 102197
- F. Zhang, C.-A. Di, N. Berdunov, Y. Hu, Y. Hu et al., Ultrathin film organic transistors: precise control of semiconductor thickness *via* spin-coating. Adv. Mater. 25(10), 1401–1407 (2013). https://doi.org/10.1002/adma.201204075
- A.M. Glaudell, J.E. Cochran, S.N. Patel, M.L. Chabinyc, Impact of the doping method on conductivity and thermopower in semiconducting polythiophenes. Adv. Energy Mater. 5(4), 1401072 (2015). https://doi.org/10.1002/aenm. 201401072
- X. Mu, W. Wang, C. Sun, D. Zhao, C. Ma et al., Greatly increased electrical conductivity of PBTTT-C14 thin film *via* controllable single precursor vapor phase infiltration. Nanotechnology 34(1), 015709 (2023). https://doi.org/10.1088/1361-6528/ac96fa
- 73. J. Kim, D. Ju, S. Kim, K. Cho, Disorder-controlled efficient doping of conjugated polymers for high-performance organic thermoelectrics. Adv. Funct. Mater. **34**(6), 2309156 (2024). https://doi.org/10.1002/adfm.202309156
- 74. O. Zapata-Arteaga, S. Marina, G. Zuo, K. Xu, B. Dörling et al., Design rules for polymer blends with high thermoelectric performance. Adv. Energy Mater. **12**(19), 2104076 (2022). https://doi.org/10.1002/aenm.202104076
- 75. V. Vijayakumar, Y. Zhong, V. Untilova, M. Bahri, L. Herrmann et al., Bringing conducting polymers to high order: toward conductivities beyond 105 S cm<sup>-1</sup> and thermoelectric power factors of 2 mW m<sup>-1</sup> K<sup>-2</sup>. Adv. Energy Mater. 9(24), 1900266 (2019). https://doi.org/10.1002/aenm. 201900266
- M. Pandey, S.S. Pandey, S. Nagamatsu, S. Hayase, W. Takashima, Solvent driven performance in thin floating-films of PBTTT for organic field effect transistor: role of macroscopic orientation. Org. Electron. 43, 240–246 (2017). https://doi.org/10.1016/j.orgel.2017.01.031

- 77. M. Pandey, J. Toyoda, S. Sharma, Y. Cho, H. Benten et al., The role of solvents in the microstructure and charge transport of semiconducting polymer films prepared at the air—liquid interface. J. Mater. Chem. C **11**(36), 12364–12373 (2023). https://doi.org/10.1039/D3TC02282J
- 78. A. Dauendorffer, S. Miyajima, S. Nagamatsu, W. Takashima, S. Hayase et al., One-step deposition of self-oriented β-phase polyfluorene thin films for polarized polymer light-emitting diodes. Appl. Phys. Express 5(9), 092101 (2012). https://doi.org/10.1143/apex.5.092101
- 79. M. Ito, Y. Yamashita, T. Mori, M. Chiba, T. Futae et al., Hyper 100 °C Langmuir–blodgett (Langmuir–schaefer) technique for organized ultrathin film of polymeric semiconductors. Langmuir 38(17), 5237–5247 (2022). https://doi.org/10.1021/acs.langmuir.1c02596
- Y.-S. Kim, H. Kim, T. Yoon, M.-J. Kim, J. Lee et al., Latent and controllable doping of stimuli-activated molecular dopants for flexible and printable organic thermoelectric generators. Chem. Eng. J. 470, 144129 (2023). https://doi. org/10.1016/j.cej.2023.144129
- N. Yousefi, R.D. Pettipas, T.L. Kelly, L.G. Kaake, Self-assembly of PBTTT-C<sub>14</sub> thin films in supercritical fluids. Mater. Adv. 3(5), 2515–2523 (2022). https://doi.org/10.1039/dlma00847a
- H. Zeng, P. Durand, S. Guchait, L. Herrmann, C. Kiefer et al., Optimizing chain alignment and preserving the pristine structure of single-ether based PBTTT helps improve thermoelectric properties in sequentially doped thin films. J. Mater. Chem. C 10(42), 15883–15896 (2022). https://doi.org/10.1039/D2TC03600B
- 83. P. Limelette, N. Leclerc, M. Brinkmann, Heterogeneous oriented structure model of thermoelectric transport in conducting polymers. Sci. Rep. **13**(1), 21161 (2023). https://doi.org/10.1038/s41598-023-48353-5
- 84. S.N. Patel, A.M. Glaudell, K.A. Peterson, E.M. Thomas, K.A. O'Hara et al., Morphology controls the thermoelectric power factor of a doped semiconducting polymer. Sci. Adv. 3(6), e1700434 (2017). https://doi.org/10.1126/sciady.1700434
- 85. Y. Yamashita, J. Tsurumi, M. Ohno, R. Fujimoto, S. Kumagai et al., Efficient molecular doping of polymeric semiconductors driven by anion exchange. Nature **572**(7771), 634–638 (2019). https://doi.org/10.1038/s41586-019-1504-9
- B. Yurash, D.X. Cao, V.V. Brus, D. Leifert, M. Wang et al., Towards understanding the doping mechanism of organic semiconductors by Lewis acids. Nat. Mater. 18(12), 1327– 1334 (2019). https://doi.org/10.1038/s41563-019-0479-0
- 87. N. Chen, T. Mukhopadhyay, Y. Song, S. Griggs, C.J. Kousseff et al., Enhancing electrical conductivity and power factor in poly-glycol-bithienylthienothiophene with oligoethylene glycol side chains through tris (pentafluorophenyl) borane doping. Adv. Funct. Mater. **34**(33), 2400469 (2024). https://doi.org/10.1002/adfm.202400469
- A. Dash, S. Guchait, D. Scheunemann, V. Vijayakumar, N. Leclerc et al., Spontaneous modulation doping in semi-crystalline conjugated polymers leads to high conductivity at low





doping concentration. Adv. Mater. **36**(13), 2311303 (2024). https://doi.org/10.1002/adma.202311303

N.J. Pataki, S. Guchait, B. Jismy, N. Leclerc, A. Kyndiah et al., A label-like monolithic organic thermoelectric generator enabled by local inkjet doping of aligned polymer films (Adv. Energy Mater. 15/2025). Adv. Energy Mater. 15(15), 2570076 (2025). https://doi.org/10.1002/aenm.202570076

82

- S. Guchait, S. Oummouch, P. Durand, N. Kamatham, B. Jismy et al., Impact of side chain chemical structure on doping and thermoelectric properties of oriented PBTTT thin films. Small 21(6), 2410073 (2025). https://doi.org/10.1002/smll.202410073
- X.-Y. Deng, Z. Zhang, T. Lei, Integrated materials design and process engineering for n-type polymer thermoelectrics. JACS Au 4(11), 4066–4083 (2024). https://doi.org/10.1021/ jacsau.4c00638
- 92. H. Tanaka, S.-I. Ito, T. Matsui, T. Takenobu, Facile and controllable chemical doping of conducting polymers with an ionic liquid dopant. Appl. Phys. Express 17(3), 031002 (2024). https://doi.org/10.35848/1882-0786/ad2f66
- I.E. Jacobs, Y. Lin, Y. Huang, X. Ren, D. Simatos et al., Highefficiency ion-exchange doping of conducting polymers. Adv. Mater. 34(22), 2102988 (2022). https://doi.org/10.1002/adma.202102988
- C. Chen, I.E. Jacobs, K. Kang, Y. Lin, C. Jellett et al., Observation of weak counterion size dependence of thermoelectric transport in ion exchange doped conducting polymers across a wide range of conductivities. Adv. Energy Mater. 13(9), 2202797 (2023). https://doi.org/10.1002/aenm.202202797
- 95. W. Jin, C.-Y. Yang, R. Pau, Q. Wang, E.K. Tekelenburg et al., Photocatalytic doping of organic semiconductors. Nature **630**(8015), 96–101 (2024). https://doi.org/10.1038/s41586-024-07400-5
- 96. V. Vijayakumar, P. Durand, H. Zeng, V. Untilova, L. Herrmann et al., Influence of dopant size and doping method on the structure and thermoelectric properties of PBTTT films doped with F<sub>6</sub>TCNQ and F<sub>4</sub>TCNQ. J. Mater. Chem. C 8(46), 16470–16482 (2020). https://doi.org/10.1039/D0TC02828B
- V. Vijayakumar, E. Zaborova, L. Biniek, H. Zeng, L. Herrmann et al., Effect of alkyl side chain length on doping kinetics, thermopower, and charge transport properties in highly oriented F<sub>4</sub>TCNQ-doped PBTTT films. ACS Appl. Mater. Interfaces 11(5), 4942–4953 (2019). https://doi.org/10.1021/acsami.8b17594
- 98. Z. Jia, W. Wang, C. Ma, X. Zhang, R. Yan et al., Efficiently tuning the electrical performance of PBTTT-C14 thin film viainsitucontrollable multiple precursors (Al<sub>2</sub>O<sub>3</sub>: ZnO) vapor phase infiltration. Nanotechnology (2024). https://doi.org/10. 1088/1361-6528/ad375c
- C.Z. Leng, M.D. Losego, Vapor phase infiltration (VPI) for transforming polymers into organic-inorganic hybrid materials: a critical review of current progress and future challenges. Mater. Horiz. 4(5), 747–771 (2017). https://doi.org/ 10.1039/C7MH00196G
- I. Azpitarte, M. Knez, Vapor phase infiltration: from a bioinspired process to technologic application, a prospective

- review. MRS Commun. **8**(3), 727–741 (2018). https://doi.org/10.1557/mrc.2018.126
- I.E. Jacobs, A.J. Moulé, Controlling molecular doping in organic semiconductors. Adv. Mater. 29(42), 1703063 (2017). https://doi.org/10.1002/adma.201703063
- 102. I. Salzmann, G. Heimel, M. Oehzelt, S. Winkler, N. Koch, Molecular electrical doping of organic semiconductors: fundamental mechanisms and emerging dopant design rules. Acc. Chem. Res. 49(3), 370–378 (2016). https://doi.org/10. 1021/acs.accounts.5b00438
- Y. Li, C.-Y. Gao, X.-H. Fan, L.-M. Yang, *In-situ* pulse electropolymerization of pyrrole on single-walled carbon nanotubes for thermoelectric composite materials. Chem. Eng. J. 443, 136536 (2022). https://doi.org/10.1016/j.cej.2022. 136536
- 104. Y. Bao, Y. Sun, F. Jiao, W. Hu, Recent advances in multicomponent organic composite thermoelectric materials. Adv. Electron. Mater. 9(5), 2201310 (2023). https://doi.org/10.1002/aelm.202201310
- J. Liu, J. Moo-Young, M. McInnis, M.A. Pasquinelli, L. Zhai, Conjugated polymer assemblies on carbon nanotubes. Macromolecules 47(2), 705–712 (2014). https://doi.org/10.1021/ma401609q
- 106. S.H. Kim, S. Jeong, D. Kim, C.Y. Son, K. Cho, Effects of connecting polymer structure and morphology at inter-tube junctions on the thermoelectric properties of conjugated polymer/carbon nanotube composites. Adv. Electron. Mater. 9(7), 2201293 (2023). https://doi.org/10.1002/aelm.202201293
- 107. P.K. Sahu, R.K. Pandey, R. Dwivedi, V.N. Mishra, R. Prakash, Polymer/Graphene oxide nanocomposite thin film for NO<sub>2</sub> sensor: an *in situ* investigation of electronic, morphological, structural, and spectroscopic properties. Sci. Rep. 10, 2981 (2020). https://doi.org/10.1038/s41598-020-59726-5
- O. Zapata-Arteaga, A. Perevedentsev, S. Marina, J. Martin, J.S. Reparaz et al., Reduction of the lattice thermal conductivity of polymer semiconductors by molecular doping. ACS Energy Lett. 5(9), 2972–2978 (2020). https://doi.org/10.1021/acsenergylett.0c01410
- X. Rodríguez-Martínez, F. Saiz, B. Dörling, S. Marina, J. Guo et al., On the thermal conductivity of conjugated polymers for thermoelectrics. Adv. Energy Mater. 14(35), 2401705 (2024). https://doi.org/10.1002/aenm.202401705
- 110. Z.-F. Yao, J.-Y. Wang, J. Pei, Controlling morphology and microstructure of conjugated polymers *via* solution-state aggregation. Prog. Polym. Sci. **136**, 101626 (2023). https://doi.org/10.1016/j.progpolymsci.2022.101626
- 111. L. Xu, H. Zhang, Y. Lu, L. An, T. Shi, The effects of solvent polarity on the crystallization behavior of thin  $\pi$ -conjugated polymer film in solvent mixtures investigated by grazing incident X-ray diffraction. Polymer **190**, 122259 (2020). https://doi.org/10.1016/j.polymer.2020.122259
- 112. J. Zhou, Y. Wang, X. Hao, C. Ma, Y. Wang et al., Controllable conformation transfer of conjugated polymer toward high photoelectrical performance: the role of solvent in induced-crystallization route. J. Phys. Chem. C 122(2), 1037–1043 (2018). https://doi.org/10.1021/acs.jpcc.7b09324

Nano-Micro Lett. (2026) 18:82 Page 33 of 34 82

- 113. L.-H. Zhao, R.-Q. Png, J.-M. Zhuo, L.-Y. Wong, J.-C. Tang et al., Role of borderline solvents to induce pronounced extended-chain lamellar order in π-stackable polymers. Macromolecules **44**(24), 9692–9702 (2011). https://doi.org/10.1021/ma201165y
- 114. A.M. Gaikwad, Y. Khan, A.E. Ostfeld, S. Pandya, S. Abraham et al., Identifying orthogonal solvents for solution processed organic transistors. Org. Electron. 30, 18–29 (2016). https://doi.org/10.1016/j.orgel.2015.12.008
- 115. H.L. Yi, C.H. Wu, C.I. Wang, C.C. Hua, Solvent-regulated mesoscale aggregation properties of dilute PBTTT-C<sub>14</sub> solutions. Macromolecules **50**(14), 5498–5509 (2017). https://doi.org/10.1021/acs.macromol.7b00790
- C. Liu, W. Yang, H. Jiang, B. Zhang, G. Liu et al., Chain conformation and liquid-crystalline structures of a poly(thieno) thiophene. Macromolecules 55(7), 2892–2903 (2022). https://doi.org/10.1021/acs.macromol.2c00143
- 117. A.K. Diallo, A.K. Diallo, R. Ndioukane, N.C.Y. Fall, A. Tall et al., Influence of solvents on the electrical parameters of poly(2, 5-bis(3-alkylthiophen-2-yl)thieno [3, 2-b] thiophene) (PBTTT) field effect transistor. MRS Adv. 8(13), 723–728 (2023). https://doi.org/10.1557/s43580-023-00577-3
- 118. G. Ma, Z. Li, L. Fang, W. Xia, X. Gu, Effect of solvent quality and sidechain architecture on conjugated polymer chain conformation in solution. Nanoscale 16(13), 6495–6506 (2024). https://doi.org/10.1039/D3NR05721F
- A. Gasperini, K. Sivula, Effects of molecular weight on microstructure and carrier transport in a semicrystalline poly(thieno)thiophene. Macromolecules 46(23), 9349–9358 (2013). https://doi.org/10.1021/ma402027v
- 120. Q. Zhao, H. Zheng, D. Li, J. Peng, Interrogating cocrystallization and microphase segregation in meticulously engineered rod–rod poly(thieno)thiophene-based block copolymers for organic field-effect transistors. Macromolecules 57(10), 4782–4792 (2024). https://doi.org/10.1021/acs.macromol. 4c00632
- Q. Zhao, D. Li, J. Peng, Interrogating polymorphism in conjugated poly(thieno)thiophene thin films for field-effect transistors. Macromolecules 56(2), 490–500 (2023). https://doi.org/10.1021/acs.macromol.2c02289
- 122. W. Zhu, X. Qiu, J.E.M. Laulainen, H.-L. Un, X. Ren et al., Enhancing the conductivity and thermoelectric performance of semicrystalline conducting polymers through controlled tie chain incorporation. Adv. Mater. 36(28), 2310480 (2024). https://doi.org/10.1002/adma.202310480
- 123. C.-H. Tsai, Y.-C. Lin, W.-N. Wu, S.-H. Tung, W.-C. Chen et al., Optimizing the doping efficiency and thermoelectric properties of isoindigo-based conjugated polymers using side chain engineering. J. Mater. Chem. C 11(21), 6874–6883 (2023). https://doi.org/10.1039/D3TC00883E
- 124. S.E. Yoon, S.J. Shin, S.Y. Lee, G.G. Jeon, H. Kang et al., Strategic side-chain engineering approach for optimizing thermoelectric properties of isoindigo-based conjugated polymers. ACS Appl. Polym. Mater. 2(7), 2729–2735 (2020). https://doi.org/10.1021/acsapm.0c00332

- 125. E.H. Suh, M.-K. Jeong, K. Lee, W. Jeong, Y.J. Jeong et al., Understanding the solution-state doping of donor–acceptor polymers through tailored side chain engineering for thermoelectrics. Adv. Funct. Mater. 32(51), 2207886 (2022). https:// doi.org/10.1002/adfm.202207886
- 126. Q. Zhao, D. Li, J. Peng, Meticulous molecular engineering of crystal orientation and morphology in conjugated polymer thin films for field-effect transistors. ACS Appl. Mater. Interfaces 16(7), 9098–9107 (2024). https://doi.org/10.1021/ acsami.3c16192
- 127. P. Durand, H. Zeng, T. Biskup, V. Vijayakumar, V. Untilova et al., Single ether-based side chains in conjugated polymers: toward power factors of 2.9 mW m<sup>-1</sup> K<sup>-2</sup>. Adv. Energy Mater. **12**(2), 2103049 (2022). https://doi.org/10.1002/aenm. 202103049
- 128. K.G. Cho, D.Z. Adrahtas, K.H. Lee, C.D. Frisbie, Sub-band filling and hole transport in polythiophene-based electrolytegated transistors: effect of side-chain length and density. Adv. Funct. Mater. **33**(37), 2303700 (2023). https://doi.org/10.1002/adfm.202303700
- 129. L. Zhang, H. Li, K. Zhao, T. Zhang, D. Liu et al., Improving crystallinity and ordering of PBTTT by inhibiting nematic to smectic phase transition *via* rapid cooling. Polymer **256**, 125178 (2022). https://doi.org/10.1016/j.polymer.2022. 125178
- 130. T. Qu, Y. Li, L. Li, C. Zhang, X. Wang et al., Monitoring molecular ordering of a conjugated polymer: PBTTT during conformational evolution. Macromolecules 56(16), 6407– 6418 (2023). https://doi.org/10.1021/acs.macromol.3c00709
- 131. V. Pirela, A.J. Müller, J. Martín, Crystallization kinetics of semiconducting poly(2, 5-bis(3-alkylthiophen-2-yl)-thieno-[3, 2-*b*] thiophene) (PBTTT) from its different liquid phases. J. Mater. Chem. C **12**(11), 4005–4012 (2024). https://doi.org/10.1039/d3tc03850e
- 132. M. Ishii, Y. Yamashita, S. Watanabe, K. Ariga, J. Takeya, Doping of molecular semiconductors through proton-coupled electron transfer. Nature 622(7982), 285–291 (2023). https:// doi.org/10.1038/s41586-023-06504-8
- 133. L. Xiang, Z. He, C. Yan, Y. Zhao, Z. Li et al., Nanoscale doping of polymeric semiconductors with confined electrochemical ion implantation. Nat. Nanotechnol. 19(8), 1122–1129 (2024). https://doi.org/10.1038/s41565-024-01653-x
- 134. Q. Zhang, Y. Sun, F. Jiao, J. Zhang, W. Xu et al., Effects of structural order in the pristine state on the thermoelectric power-factor of doped PBTTT films. Synth. Met. 162(9–10), 788–793 (2012). https://doi.org/10.1016/j.synthmet.2012.03. 003
- 135. Q. Zhang, Y. Sun, W. Xu, D. Zhu, What to expect from conducting polymers on the playground of thermoelectricity: lessons learned from four high-mobility polymeric semiconductors. Macromolecules 47(2), 609–615 (2014). https://doi.org/10.1021/ma4020406
- 136. H. Li, E. Plunkett, Z. Cai, B. Qiu, T. Wei et al., Dopant-dependent increase in seebeck coefficient and electrical conductivity in blended polymers with offset carrier energies.





- Adv. Electron. Mater. **5**(11), 1800618 (2019). https://doi.org/10.1002/aelm.201800618
- 137. X. Chen, J. Jin, S. Sun, H. Xiao, L. Wang et al., Thickness-dependent thermoelectric properties of ultrathin polymer film on self-assembled monolayers. Appl. Phys. Lett. 124(8), 083903 (2024), https://doi.org/10.1063/5.0192020
- 138. C. Chen, H. Ma, K. Lu, X. Zhang, B. Yue et al., Boosting thermoelectric performance of semicrystalline conducting polymers by simply adding nucleating agent. Adv. Mater. 37(9), 2417594 (2025). https://doi.org/10.1002/adma.20241 7594
- M. Cutler, N.F. Mott, Observation of anderson localization in an electron gas. Phys. Rev. 181(3), 1336–1340 (1969). https:// doi.org/10.1103/physrev.181.1336
- 140. X. Guan, W. Feng, X. Wang, R. Venkatesh, J. Ouyang, Significant enhancement in the seebeck coefficient and power factor of p-type poly(3, 4-ethylenedioxythiophene): poly(styrenesulfonate) through the incorporation of n-type MXene. ACS Appl. Mater. Interfaces 12(11), 13013–13020 (2020). https://doi.org/10.1021/acsami.9b21185
- 141. D. Kim, J. Kim, S. Chung, K. Cho, Quantum-dot-induced energy filtering effect in organic thermoelectric nanocomposites. Adv. Electron. Mater. **10**(9), 2300814 (2024). https://doi.org/10.1002/aelm.202300814

- 142. G. Yang, B.-Y. Cao, Three-sensor 3ω-2ω method for the simultaneous measurement of thermal conductivity and thermal boundary resistance in film-on-substrate heterostructures. J. Appl. Phys. **133**(4), 045104 (2023). https://doi.org/10.1063/5.0120284
- 143. G. Yang, B.-Y. Cao, Three-sensor 2ω method with multi-directional layout: a general methodology for measuring thermal conductivity of solid materials. Int. J. Heat Mass Transf. **219**, 124878 (2024). https://doi.org/10.1016/j.ijheatmasstransfer.2023.124878
- 144. K. Takayama, G. Ito, S. Kanazawa, R. Ikkatai, K. Noda, Cross-plane thermal transport in acceptor-doped thiophenebased polymer thin films investigated by the 3-omega method. Phys. Status Solidi A 220(24), 2300110 (2023). https://doi. org/10.1002/pssa.202300110
- 145. Y. Zhang, R. Xu, Y. Liu, Q. Jiang, Q. Li et al., Anisotropic thermal diffusivity measurement of thin films: from a few to hundreds of microns. Int. J. Heat Mass Transf. 227, 125536 (2024). https://doi.org/10.1016/j.ijheatmasstransfer.2024. 125536

**Publisher's Note** Springer Nature remains neutral with regard to jurisdictional claims in published maps and institutional affiliations.